Antagonist Analogue of 6-[3′-(1-Adamantyl)-4′-hydroxyphenyl]-2-naphthalenecarboxylic Acid (AHPN) Family of Apoptosis Inducers That Effectively Blocks AHPN-Induced Apoptosis but Not Cell-Cycle Arrest

Marcia I. Dawson,*,† Danni L. Harris,§ Gang Liu,† Peter D. Hobbs,‡ Christopher W. Lange,⊗ Ling Jong,‡ Nathalie Bruey-Sedano,† Sharon Y. James,† Xiao-kun Zhang,† Valerie J. Peterson,# Mark Leid,# Lulu Farhana,||,▽ Arun K. Rishi,|| and Joseph A. Fontana||,▽

The Burnham Institute, Cancer Center, 10901 North Torrey Pines Road, La Jolla, California 92037; Molecular Research Institute, 2495 Old Middlefield Road, Mountain View, California 94043; SRI International, Retinoid Program, 333 Ravenswood Avenue, Menlo Park, California 94025; Oregon State University, College of Pharmacy, Corvallis, Oregon 97331; and Wayne State University and John D. Dingell Medical Center, Department of Veterans Affairs, 4646 John R Street, Detroit, Michigan 48201

Received October 15, 2003

The retinoid 6-[3′-(1-adamantyl)-4′-hydroxyphenyl]-2-naphthalenecarboxylic acid (AHPN) and its active analogues induce cell-cycle arrest and programmed cell death (apoptosis) in cancer cells independently of retinoic acid receptor (RAR) interaction. Its analogue, (*E*)-4-[3′-(1-adamantyl)-4′-hydroxyphenyl]-3-(3′-acetamidopropyloxy)cinnamic acid (3-A-AHPC) selectively antagonized cell apoptotic events (TR3/nur77/NGFI-B expression and nuclear-to-mitochondrial translocation) but not the proliferative events (cell-cycle arrest and $p21^{WAF1/CIP1}$ expression) induced by proapoptotic AHPN and its analogues. The syntheses of 3-A-AHPC and proapoptotic (*E*)-6-[3′-(1-adamantyl)-4′-hydroxyphenyl]-5-chloronaphthalenecarboxylic acid (5-Cl-AHPN) are described. Computational studies on AHPN, AHPC, and three substituted analogues (5-Cl-AHPN, 3-Cl-AHPC, and 3-A-AHPC) suggested reasons for their diametric effects on RAR activation. Density functional theory studies indicated that the 1-adamantyl (1-Ad) groups of the AHPN and AHPC configurations assumed positions that were nearly planar with the aromatic rings of their polar termini. In contrast, in the configurations of the substituted analogues having chloro and 3-acetamidopropyloxy groups, rather than a hydrogen, ortho to the diaryl bonds, the diaryl bond torsion angles increased so that the 1-Ad groups were oriented out of this plane. Docking and molecular dynamics of AHPN, AHPC, and these substituted analogues in the RARγ ligand-binding domain illustrated how specific substituents on the AHPN and AHPC scaffolds modulated the positions and dynamics of the 1-Ad groups. As a result, the position of RARγ helix H12 in forming the coactivator-binding site was impacted in a manner consistent with the experimental effect of each analogue on RARγ transcriptional activation.

Introduction

Previously, we established that the retinoid 6-[3′-(1-adamantyl)-4′-hydroxyphenyl]-2-naphthalenecarboxylic acid (CD437[1]/AHPN, **1** in Figure 1) inhibited cancer cell growth and induced cancer cell apoptosis (programmed cell death) by signaling pathways that did not involve the direct interaction of AHPN with the retinoic acid receptor subtypes (RARs) α, β, and γ,[2−5] which function as nuclear transcription factors.[6] AHPN was first reported as an RARγ-selective retinoid.[1] Earlier, Dawson and co-workers had observed that the levels of MCF-7 anchorage-dependent cell growth inhibition by retinoids positively correlated with their abilities to interact with RARα, whereas their inhibition of anchorage-independent (clonal) growth only correlated with their transcriptional activation of RARα.[7] Fitzgerald and co-workers extended these observations of the correlation between growth inhibition by retinoids and RARα activation to other breast cancer cell lines.[8] Our inability to observe a correlation between the inhibition of ovarian cancer cell growth and RAR subtype activation by AHPN and its analogues (AHPNs)[9] underscored our hypothesis that AHPN signaling in cancer cells occurred through a pathway that did not involve the activation of RARs by this new class of apoptosis-inducing agents. Although the signaling pathway by which AHPN and its analogues initiate apoptosis remains to be fully elucidated, we found[10] that it involved the intrinsic apoptotic pathway of mitochondrial membrane potential change, mitochondrial cytochrome *c* release into the cytosol, followed by the binding of cytochrome *c* to the apaf-12 complex that, in turn, activated procaspase-9. The activated enzyme initiated a caspase cascade of cell degradation that included irreversible morphological

* To whom correspondence should be addressed. Phone: 858-646-3165. Fax: 858-646-3197. E-mail: mdawson@burnham.org.
† The Burnham Institute.
§ Molecular Research Institute.
‡ SRI International.
|| Wayne State University.
▽ Department of Veterans Affairs.
Oregon State University.
⊗ Current address: Discovery Partners International, Chem. RX Division, 385 Oyster Point Blvd., South San Francisco, CA 94080.

10.1021/jm030524k CCC: $27.50
Published on Web 06/05/2004

changes, DNA cleavage, nuclear fragmentation, and other processes indicative of apoptosis.

Our efforts to define this pathway led to the further discovery of a novel paradigm[10] for the extranuclear behavior of the nuclear receptor TR3/nur77/NGFI-B (human/mouse/rat TR3)[11−13] and retinoid X receptor (RXR)[14] that, like the RARs, functions in the nucleus as a transcription factor. We established that AHPN and its analogues induced the expression of TR3 and its migration from the nucleus to mitochondria,[10] where TR3 modulated the function of the anti-apoptotic protein Bcl-2, which typically protects mitochondria from apoptotic insults.[15] On interacting with TR3, Bcl-2 was no longer able to protect the cell from apoptosis but underwent a conformational change that promoted apoptosis.[16] We also discovered that chemotherapeutic drugs, such as etoposide, were able to induce prostate cancer cell apoptosis through this pathway.[10]

An apoptotic signaling pathway for the AHPNs that does not involve typical RAR signaling is actually advantageous. The retinoids currently approved for the treatment of cancer and other proliferative diseases—*all-trans*-retinoic acid (*trans*-RA, **4**), 9-*cis*-RA (**5**), 13-*cis*-RA, and Targretin/bexarotene (**6**)—have adverse effects.[17−29] In retinoid-treated patients, these effects have included hypertriglyceridemia leading to pancreatitis, pseudotumor cerebri, RA syndrome (respiratory failure), hypothyroidism, and teratogenesis, all of which limit effective dosage and discourage compliance. Transcriptional activation of RARγ by retinoids has been reported to correlate with retinoid toxicity.[30−33] In addition, transformed cells often lose sensitivity to growth inhibition by retinoids through the loss of functional RARs, particularly RARβ, which has been thought to function as a tumor suppressor.[34−38]

Recently, we identified two new apoptotic AHPNs: 6-[3′-(1-adamantyl)-4′-hydroxyphenyl]-5-chloro-2-naphthalenecarboxylic acid (5-Cl-AHPN, **2**)[39] and (*E*)-4-[3′-(1-adamantyl)-4′-hydroxyphenyl]-3-chlorocinnamic acid (3-Cl-AHPC, **9**).[40] Herein, by using diverse computational chemistry approaches in combination with bioassay results, we present a rationale for the lack of retinoid transcriptional activity displayed by these substituted AHPN analogues. We also report the synthesis of the related antagonist, 3-(3′-acetamidopropyloxy)-AHPC (3-A-AHPC, **10**) in addition to that of the apoptosis inducer 5-Cl-AHPN. Our studies showed that 3-A-AHPN blocked the apoptotic signaling pathway induced by AHPN (**1**), 5-Cl-AHPN, and 3-Cl-AHPC in cancer cells and the binding of labeled AHPN to its putative nuclear receptor[4] without impacting the ability of AHPN and its proapoptotic analogues to induce cell-cycle arrest[2] and the expression of the cyclin-dependent kinase inhibitor p21$^{WAF1/CIP1}$.[3]

Design/Synthesis

Shortly after our observation of the apoptotic activity of AHPN (**1**),[2] we undertook the synthesis of analogues, including 5-Cl-AHPN (**2**), 3-Cl-AHPC (**9**), and AHPC (**11**), with the goal of removing retinoid activity to reduce any adverse effects that would be associated with transcriptional activation of the RARs. We elected to focus on the *E*-cinnamic acid scaffold of AHPC for two reasons. First, synthetic precursors to substituted cinnamic acids were far more readily available than those for similarly substituted naphthalenecarboxylic acids. Second, we hypothesized that by replacing the naphthalenecarboxylic acid moiety of AHPN with a cinnamic acid group we would reduce retinoid activity. Prior to 1990, we had synthesized the cinnamic acid **15**[41] as an analogue of the retinoid TTNN (**16**).[42] This strategy was not particularly useful for retinoid design as evidenced by the two-log higher EC_{50} value determined for **15** in reversing the keratinization of vitamin A-deficient tracheal epithelium in organ culture (TOC assay) compared to that of TTNN.[41] We subsequently found that the activity of retinoids in the TOC assay[41,43] correlated with their ability to transcriptionally activate the RARs bound to their RA-responsive elements (RAREs) in the promoter regions of retinoid-responsive genes. There-

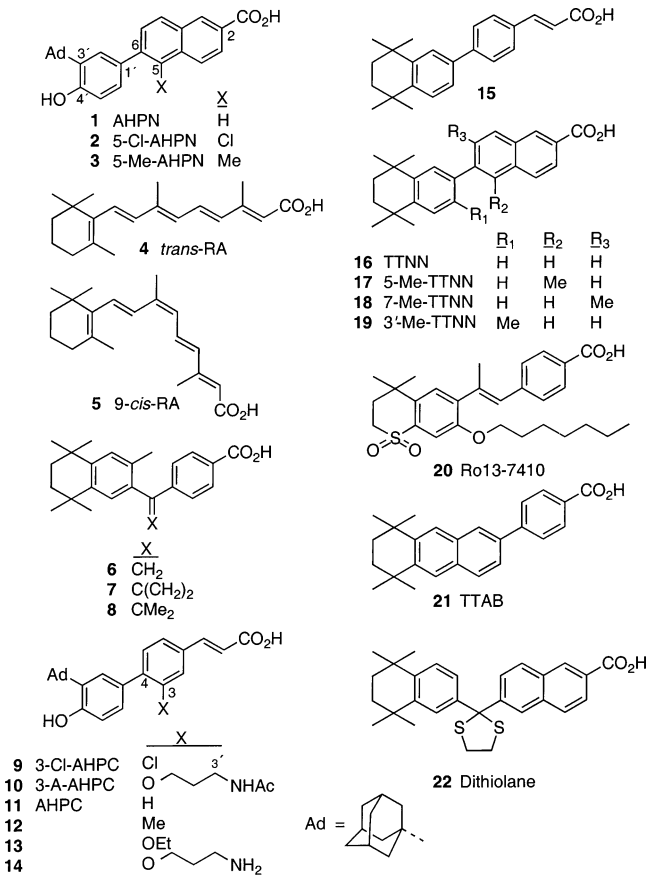

Figure 1. 6-[3′-(1-Adamantyl)-4′-hydroxyphenyl]-2-naphthalenecarboxylic acid (AHPN, **1**); AHPN analogues 5-chloro-AHPN (5-Cl-AHPN, **2**) and 5-methyl-AHPN (5-Me-AHPN, **3**); retinoic acid receptor (RAR)-selective agonist *trans*-retinoic acid (*trans*-RA, **4**); RAR and retinoid X receptor (RXR) panagonist 9-*cis*-retinoic acid (9-*cis*-RA, **5**); RXR-selective retinoids Targretin (11247, **6**), 11173 (**7**), and 11345 (**8**); (*E*)-4-[3′-(1-adamantyl)-4′-hydroxyphenyl]cinnamic acid (AHPC, **11**); AHPC analogues 3-chloro-AHPC (3-Cl-AHPC, **9**), 3-(3′-acetamidopropyloxy)-AHPC (3-A-AHPC, **10**), 3-Me-AHPC (**12**), 3-EtO-AHPC (**13**), and 3-(3′-aminopropyloxy)-AHPC (**14**); RARβ,γ-selective (*E*)-4-(5′,6′,7′,8′-tetrahydro-5′,5′,8′,8′-tetramethyl-2′-naphthalenyl)cinnamic acid (**15**), 6-(5′,6′,7′,8′-tetrahydro-5′,5′,8′,8′-tetramethyl-2′-naphthalenyl)-2-naphthalenecarboxylic acid (TTNN, **16**), 5-Me-TTNN (**17**), 7-Me-TTNN (**18**), 3′-Me-TTNN (**19**); RARα-selective antagonist Ro41-5253 (**20**); RAR-selective agonist 4-(5′,6′,7′,8′-tetrahydro-5′,5′,8′,8′-tetramethyl-2′-anthracenyl)benzoic acid (TTAB, **21**); and RARγ-selective antagonist 2-(5′,6′,7′,8′-tetrahydro-5′,5′,8′,8′-tetramethyl-2′-naphthalenyl)-2-(6′-carboxynaphthalene)-1,3-dithiolane (11253, **22**).

Table 1. Cancer Cell Apoptosis and Growth Inhibition Activities Induced by AHPN, AHPC, and Analogues Compared to Their Calculated Inter-Ring Dihedral Angles

	apoptosis (%)[a]				growth inhibition (%)[b]		
	HL-60R (24 h)		MDA-MB-231 (96 h)		H460 (144 h)		
analogue	0.1×10^{-6} M	1.0×10^{-6} M	0.5×10^{-6} M	1.0×10^{-6} M	0.1×10^{-6} M	1.0×10^{-6} M	angle[c] (deg)
AHPN (**1**)	78	98	26	46	20	80	31
5-Me-AHPN (**3**)	29	70	14	–	–	–	29
AHPC (**11**)	90	98	53	58	–	–	21
3-Me-AHPC (**12**)	10	95	5	30	–	–	–
3-EtO-AHPC (**13**)	0	29	–[d]	–	14	52	–
5-Cl-AHPN (**2**)	62	94	21	41	56	71	61
3-Cl-AHPC (**9**)	51	94	31	43	–	–	51
3-A-AHPC (**10**)	0	0	0	1	–	–	70

[a] Average of triplicates ± ≤ 10% for HL-60R leukemia and MDA-MB-231 breast cancer apoptosis as determined by acridine orange staining. [b]Average of triplicates ± ≤10% for H460 lung cancer apoptosis as determined by DAPI staining. [c]AHPN scaffold 5−6−1′−2′ or AHPC scaffold 3−4−1′−2′ dihedral angle determined by AM1. [d]Not determined.

fore, we rationalized that AHPC, the cinnamic acid analogue of AHPN, would have comparably reduced retinoid agonist activity. This hypothesis only held for the activation of RARα by AHPC. Transcriptional activations of RAR subtypes α, *β*, and *γ* on the $(TREpal)_2$-*tk*-CAT reporter induced by 1.0×10^{-6} M AHPC were 8%, 85%, and 103%, respectively, whereas those induced by 1.0×10^{-6} M AHPN were 21%, 78%, and 88%. Fortunately, because apoptosis-inducing activity was retained by AHPC, we pursued further modifications of the AHPC scaffold. The synthesis and apoptotic activity of AHPC were recently reported by Cincinelli et al.[44]

Introducing a methyl group at the 5- or 7-naphthalene ring position of TTNN (**16**), which was ortho to the central diaryl bond, also decreased retinoid agonist activity, as was evidenced by the higher EC_{50} values for 5-Me-TTNN (**17**) and 7-Me-TTNN (**18**) in the TOC assay compared to that of TTNN.[41] The ED_{50} values for both analogues in inhibiting the induction of mouse epidermal ornithine decarboxylase (ODC) by the tumor promoter 12-*O*-tetradecanoylphorbol-13-acetate were also higher than that for TTNN.[45] As in the TOC assay, the inhibitory activities of retinoids in the ODC assay[45] correlated with their abilities to function as RAR transcriptional agonists on an RARE such as the TREpal,[46] a synthetic RE[6] used to evaluate the transcriptional activation of both RAR and retinoid X receptor (RXR) subtypes by retinoids.[47−52] The 3′-methyl analogue (**19**) of TTNN also had lower activity in the ODC assay.[45] Moreover, by introducing a 3′-methyl group onto the tetrahydrotetramethylnaphthalene (TTN) ring of a retinoid that bound RXRs to inhibit its interaction with the homologous RARs, we successfully obtained highly RXR-selective retinoids such as **6**−**8**.[51−54] The use of this strategy was also reported by other groups.[55,56] On the basis of these findings, we elected to introduce methyl groups ortho to the diaryl bridges of AHPN (**1**) and AHPC (**11**). Replacing the TTN ring of TTNN (**16**) by a 3′-(1-adamantyl)-4′-hydroxyphenyl group was also found to reduce retinoid agonist activity.[1] We combined these features in 5-Me-AHPN (**3**), which at 1.0×10^{-7} M had growth inhibitory activity approaching that of AHPN on MCF-7 and BT-20 breast cancer cells and was also not able to activate RARα. However, its activations of RAR*β* and RAR*γ* were enhanced.[57] Thus, this strategy for designing AHPNs lacking RAR transcriptional activation activity required modification.

Fortunately, further work indicated that introducing an electronegative chloro group at a position ortho to the diaryl bond on the AHPN and AHPC scaffolds satisfactorily reduced RAR activation activity. Both 5-Cl-AHPN (**2**)[39] and 3-Cl-AHPC (**9**)[40] were efficient inducers of apoptosis but had minimal ability to activate the RARs.[39,40] Therefore, a means of blocking the ability of an ANPN analogue to activate the RARs was available. Moreover, while neither *trans*-RA (**4**) nor 9-*cis*-RA (**5**) was able to displace labeled AHPN[4] from the putative AHPN receptor in HL-60R cell extracts, nonlabeled AHPN (**1**) and 5-Cl-AHPN (**2**) were effective competitive inhibitors.[4] These results provided additional evidence that AHPN and analogues such as 5-Cl-AHPN and 3-Cl-AHPC induced cancer cell apoptosis through a pathway that did not involve RAR signaling.

Because access to an antagonist would facilitate probing AHPN-signaling pathways, we also accomplished the design and synthesis of 3-A-AHPC (**10**). Its design was based on our observation that the apoptotic activities of AHPN analogues decreased as the length of their substituents at the 3-cinnamyl ring and 5-naphthyl ring positions increased without comparable decreases in their abilities to compete with tritiated AHPN for binding to the putative AHPN receptor in HL-60R leukemia and MDA-MB-468 breast cancer cell nuclear extracts.[4] HL-60R cell apoptosis induced by 24-h treatments with 1.0×10^{-6} M AHPC (**11**), 3-Me-AHPC (**12**), and 3-EtO-AHPC (**13**) was 98%, 95%, and 29% respectively, of the vehicle-alone treated control (Table 1). The Fontana group has found that this leukemia cell line was particularly convenient for assessing apoptosis induced by AHPN analogues without the interference of possible interactions with RARs. Standard retinoids such as *trans*-RA (**4**) and 9-*cis*-RA (**5**) were unable to induce apoptosis at similar concentrations because the RAR*β* and RAR*γ* proteins were absent and the RARα mutant present was dysfunctional in competently binding standard retinoids due to the deletion of its carboxyl terminus.[58] In MDA-MB-231 breast cancer cells, which were also resistant to growth inhibition by RAR-selective retinoids[2] (data not shown), 96-h treatments with 1.0×10^{-6} M AHPC and 3-Me-AHPC produced 58% and 30% apoptosis, respectively. These results also support a retinoid-independent signaling pathway for the AHPNs, as well as our findings about the impact of the substitutents ortho to their diaryl bonds on apoptosis.

Scheme 1[a]

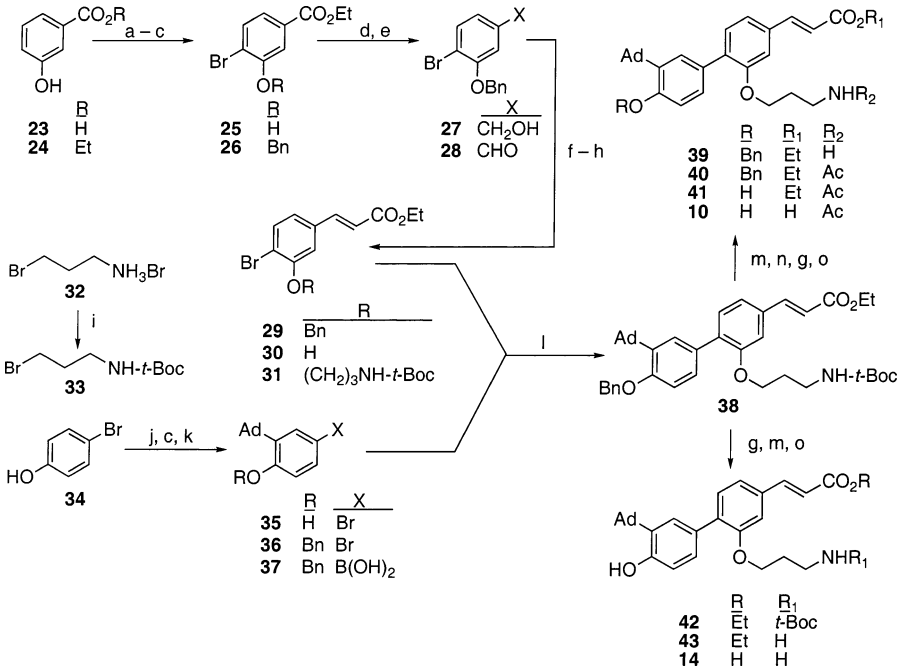

[a] (a) EtOH, $MeSO_3H$, PhH, reflux. (b) Br_2, HOAc. (c) BnBr, Na_2CO_3, Me_2CO, Et_2O/THF, −78 °C, reflux. (d) DIBAL, THF, −78 °C; H_3O^+. (e) PCC, CH_2Cl_2. (f) $[(EtO)_2P(O)CH_2CO_2Et, KN(SiMe_3)_2]$, −78° to 20 °C. (g) BBr_3, CH_2Cl_2, −78 °C; H_2O. (h) **33**, K_2CO_3, Me_2CO, reflux. (i) $(t\text{-Boc})_2O$, Et_3N, CH_2Cl_2, 0−20 °C. (j) 1-AdOH, H_2SO_4, CH_2Cl_2. (k) [*n*-BuLi, THF]; $B(Oi\text{-Pr})_3$; H_3O^+. (l) $Pd(PPh_3)_4$, aq Na_2CO_3, reflux. (m) H_3O^+, EtOH, reflux. (n) Ac_2O, py, CH_2Cl_2. (o) NaOH, MeOH, reflux; H_3O^+.

The synthesis of 3-Cl-AHPC (**9**) was previously reported by our group.[40] Antagonist 3-A-AHPC (**10**) was synthesized by a similar route, which is shown in Scheme 1. The challenge in the syntheses of 3-A-AHPC and its free amine (**14**) was the presence of three reactive groups (phenolic hydroxyl, carboxylic acid, and amide) that required selective protection and deprotection so that both compounds would be accessible from intermediate **38**. For this reason, the *tert*-butylcarbonyl group was used to protect the amine so that its removal could be achieved in the presence of both benzyl and ester protecting groups, but the amine group would remain protected during the removal of the benzyl group using boron tribromide at −78 °C. Briefly, the diaryl bond of 3-A-AHPC was introduced using a palladium(0)-catalyzed diaryl coupling of the aryl boronic acid **37**[39] with the protected (*E*)-4-bromocinnamate **31**. A three-step sequence allowed the selective removal of the protecting groups from **38**, which was immediately transformed to **10** and its related amine (**14**). The latter will be tethered to a support for use in the affinity purification of the AHPN receptor protein from HL-60R nuclear extracts.[4] The *E*-cinnamyl double bond of intermediate **29**, from which **31** was derived, was introduced by the Horner−Emmons−Wadsworth olefination of aldehyde **28** using the anion of triethyl phosphonoacetate. Isomer **29** was readily separated from a small amount (<5%) of the related *Z*-isomer by chromatography. The overall yield of the 11-step convergent sequence from **23** to **10** was 12%.

The synthesis of 5-Cl-AHPN (**2**) is outlined in Scheme 2 and resembles that reported for 3-Cl-AHPC (**9**).[40] The 5-chloro group of **46** was introduced specifically by α-chlorination of ethyl 6-hydroxy-2-naphthalenecarboxylate (**45**) using sulfuryl chloride, as had been expected because the chlorination of *β*-naphthol was reported to occur at the α-position.[59] Palladium-catalyzed diaryl coupling of triflate **47**, which was derived from **46**, with arylboronic acid **37** and deprotection provided 5-Cl-AHPN in 22% overall yield for the six steps beginning with **44**.

Scheme 2[a]

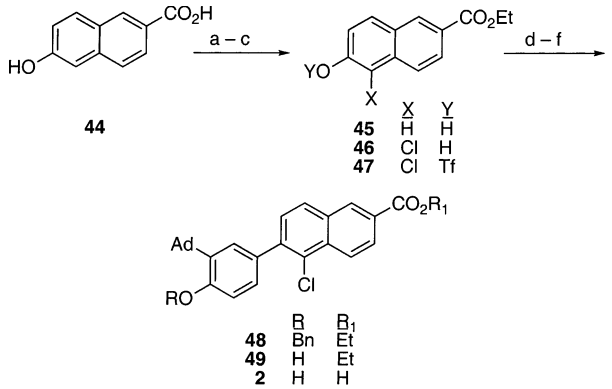

[a] (a) EtOH, H_2SO_4, reflux. (b) SO_2Cl_2, HOAc, 70 °C; H_2O. (c) $(CF_3SO_2)_2O$, pyridine, CH_2Cl_2, 0−20 °C. (d) **37**, $Pd(PPh_3)_4$, LiCl, aq Na_2CO_3, DME. (e) BBr_3, CH_2Cl_2, −78 °C; H_2O. (f) aq NaOH, EtOH, reflux; H_3O^+.

Computational Studies

Ligand Determinants of Transcriptional Activation. Often, molecular determinants that affect nuclear receptor transcriptional activation can be due to subtle effects of the ligand on receptor conformation.[60−63] Small changes in the properties of a ligand group may significantly alter either the binding mode of the ligand to the receptor or the magnitude of the interaction of the ligand with receptor binding-site residues so as to profoundly affect conformation. Our docking and molecular dynamics studies suggested that its large 3-(3′-

acetamidopropoxy) group rendered 3-A-AHPC (**10**) incapable of transcriptionally activating RARγ by preventing helix H12 from forming the coactivator-binding site. Therefore, with the binding of the coactivator protein blocked,[64] the recruitment of the multiprotein complex responsible for gene transcription could not occur.[65] The negative effect of the 3-(3′-acetamidopropoxy) group of 3-A-AHPC on RAR activation activity was not surprising because a methyl group at the 3′-position of the TTN ring enhanced the RXR selectivity of retinoids, and longer 3′-alkyl groups decreased RAR transcriptional activation in analogues of TTNN (**16**) and other retinoids.[66,67] For example, Ro-41-5253 (**20**) having a 3′-heptyloxy substituent was a potent RARα antagonist,[66] and the 3′-butyl analogue of 11173 (**7**) antagonized RXRα activation by 9-*cis*-RA (**5**).[60] Further computational probing of AHPN and AHPC analogues having similarly situated substitutents suggested that some ortho groups prevented RAR agonism by a more subtle means than by causing large changes in the LBD conformation that were distinct from those caused by AHPN (**1**). Our experimental results supported this conclusion. The ortho Cl group prevented RARβ and RARγ transcriptional activation by both 5-Cl-AHPN (**2**) and 3-Cl-AHPC (**9**). In contrast, the similarly sized 5- and 3-methyl groups of 5-Me-AHPN (**3**)[57] and 3-Me-AHPC (**12**), respectively, did not produce similar effects on RARs β and γ.

To understand why chloro group substitution ortho to the diaryl bond in AHPN analogues negatively impacted RAR activation, whereas a methyl group did not, computational studies were conducted using both the structure reported for the crystalline RARγ LBD−*trans*-RA (**4**) complex (Protein Data Bank (PDB) entry 3LBD) and small-molecule ab initio computational methods. In these studies, electron-correlation effects were included to accurately determine the torsional potential surface of each compound, which depicted how conformational energy varied as a function of torsion angle size. Because the results of density functional theory (DFT) calculations on the torsional energy barriers of substituted biphenyls[68] were in good agreement with experimental values,[69] nonlocal DFT low-energy conformations and torsional potential surfaces were determined for AHPN (**1**), 5-Cl-AHPN (**2**), 3-Cl-AHPC (**9**), 3-A-AHPC (**11**), and AHPC (**12**). The torsional potential surfaces were computed by parametrically varying the diaryl bond torsion angles while fully optimizing all other atomic positions for each step. CPK models of the optimized lowest-energy configurations of these AHPNs are illustrated in Figure 2A. The torsional potential surface for each analogue was mapped as a function of the change in the diaryl bond torsion angle 5−6−1′−2′ for AHPN and 5-Cl-AHPN and 3−4−1′−2′ for AHPC, 3-Cl-AHPC, and 3-A-AHPC, and is depicted graphically in Figure 2B. The relaxed potential surface scans indicated that the torsional potential surfaces of AHPN and AHPC were significantly different from those of the three substituted analogues. The geometry optimization and the potential surface results implied that the preferred shapes for low-energy conformations of AHPN and AHPC were more planar. Therefore, we hypothesized that if binding by a compact linear ligand was required to induce the RARγ conformation necessary for coactivator binding and transcriptional activation, the diaryl torsion angles of 5-Cl-AHPN and 3-Cl-AHPC would have been compressed to such an extent

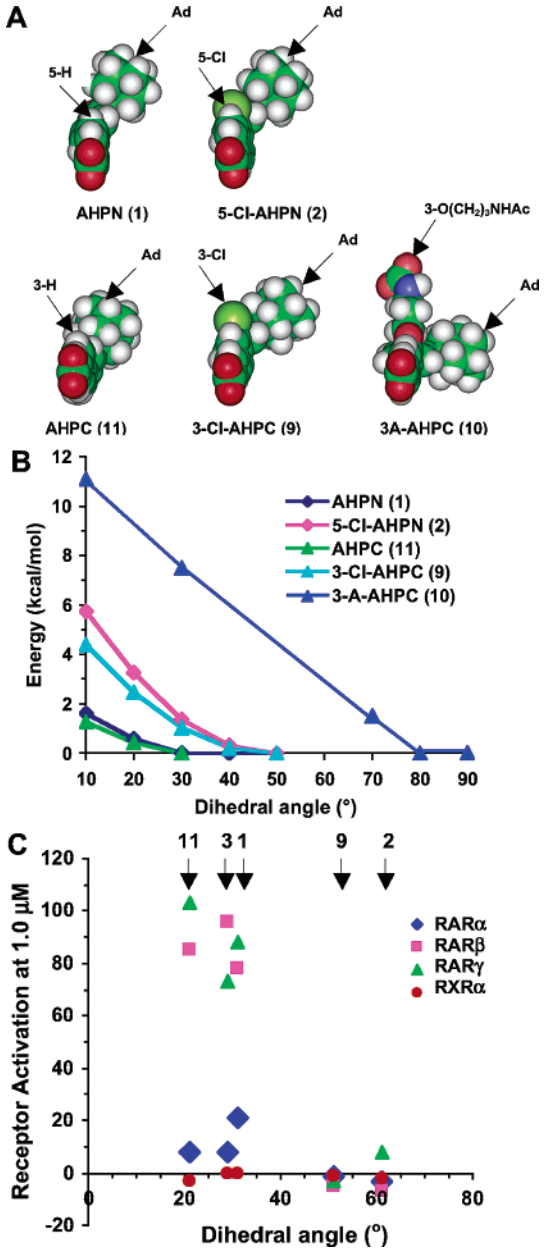

Figure 2. Ortho substituents affect the inter-ring (diaryl) bond twist in AHPN (**1**) and its analogues. A. Comparison of DFT geometry-optimized structures of AHPN and 5-Cl-AHPN (**2**) (top row), and AHPC (**11**), 3-Cl-AHPC (**9**), and 3-A-AHPC (**10**) (bottom row). Differences in inter-ring twist angles and, consequently, structure widths are depicted. Compounds are shown in space-filling format with C and Cl colored in green, O in red, N in blue, and H in white. B. Low-energy inter-ring dihedral angles reflect differences in the torsional potential surfaces of AHPN, AHPC, and their analogues that are modulated by substitutents ortho to the diaryl bond. Total energy calculated for each complex as a variable of the 5−6−1′−2′ AHPN or 5-Cl-AHPN or the 3−4−1′−2′ 3-Cl-AHPC or 3-A-AHPC torsion angle was plotted. C. Impact of substituents ortho to the diaryl bond on torsion angles of AHPN, AHPC, and their analogues and on their RARs α, β, and γ and RXRα transcriptional activation activities. Notice that on the AHPN and AHPC scaffolds that are selective for transcriptional activation of RARβ and RARγ, the chloro group had a far greater negative impact on receptor activation than a methyl group.

that the potential energies of their complexes with the RARγ LBD would have had to rise to energetically disfavored levels. Consequently, any binding by 5-Cl-AHPN and 3-Cl-AHPC to the RARγ LBD would favor 'inactive' or antagonist-like holo-receptor configurations. In Figure 2C, the negative correlation between torsional angle size and RARβ and RARγ transactivation is presented graphically for six of the analogues listed in Table 1. As shown, RXRα was not activated by these analogues, and RARα activation was very low or not existent.

We used molecular dynamics to explicitly test the hypothesis that binding of 5-Cl-AHPN (**2**) or 3-Cl-AHPC (**9**) would induce an RARγ antagonist conformation. Our results are presented in Figures 2 and 3. Docking of 5-Cl-AHPN into the RARγ ligand-binding pocket (LBP), which was obtained from the X-ray crystallographic structure of the human RARγ LBD−9-*cis*-RA (**5**) complex,[65] using the energy-based Larmarkian Genetic Algorithm (LGA) produced lowest-energy configurations in which the 5-Cl-AHPN carboxylate group interacted with the LBD helix H5 arginine-278 (Figure 3A), as had the 9-*cis*-RA carboxylate,[65] and with the hydroxyl side-chain of serine-289, which was located between the two β-sheet regions adjacent to the LBP (data not shown). The 3′-(1-adamantyl) (1-Ad) group of docked 5-Cl-AHPN nestled against the LBP hydrophobic groups of tryptophan-227 on helix H3 and those of isoleucine-412 and methionine-415 on helix H12 (Figure 3A). The 9-*cis*-RA β-cyclogeranylidene ring made similar contacts.[65] In the 5-Cl-AHPN-docking simulation, LBD helices H11 and H12 formed portions of "the roof" of the LBP, as was reported for the RARγ LBD−9-*cis*-RA complex.[65] Docking of AHPN (**1**) into the LBP yielded a low-energy binding configuration comparable to that observed for 5-Cl-AHPN (Figure 3A). These results suggested to us that the effects of the substituent ortho to the diaryl bond could not be explained by the initial configuration of the ligand docked in the holo-RARγ LBD complex but resulted from time-dependent receptor−ligand complex conformational effects.

The superposition of the 300-ps molecular dynamics configurations resulting from the simulations of the RARγ LBD complexes with AHPN (**1**) and 5-Cl-AHPN (**2**) is shown in Figure 3B. Because the docked configurations of AHPN and 5-Cl-AHPN overlapped significantly at their carboxylate termini, only 5-Cl-AHPN and the nearby LBD helical backbones in both conformations have been displayed so that backbone differences near the docked compounds were visible. While the position of the helix H10 backbone of the RARγ LBD was almost invariant in the two conformations, portions of the backbones of helices H11 (residues 393−403) and H12 (residues 410−415) adjacent to the docked compounds differed appreciably. These differences were also evident on comparing the distance-time series that tracked the AHPN and 5-Cl-AHPN−helix contact distances (Figure 3 panels C and D, respectively). Compared to the 5-hydrogen, the 5-chloro group significantly impacted the compound shape (Figure 2A) and the torsional potential surface (Figure 2B), both of which, in turn, impacted the forces on helix H12 (Figure 3A) and its conformation (Figure 3B). As a result, the time-dependent conformations of their complexes with the RARγ LBD, as reflected in the relative calculated distances between their 1-Ad carbons and the RARγ H12 isoleucine-412 backbone Cα (Figure 3C) and side-chain CD1 (Figure 3D) carbons during the periods of close contacts of each ligand with helix H12, were quite different. The time-dependence plots for the AHPN−helix H12 contact distances showed only the small fluctuations characteristic of tight or compact contacts, whereas those for the 5-Cl-AHPN−helix H12 contact distances showed the significant structural fluctuations indicative of a larger range of contact distances. These results suggested that the time-dependent dynamics of the conformations of helix H12 in the RARγ LBD when bound by AHPN or an analogue were significantly affected by the identity of the substituent ortho to the diaryl bond in AHPN and its analogues.

Initial docking of 3-A-AHPC (**10**) to the RARγ LBD produced low-energy configurations similar to those observed for 3-Cl-AHPC (**9**) for the interactions between the 3-A-AHPC carboxylate and the RARγ LBD arginine-278 and serine-289. In fact, one such docked configuration showed that the 3′-acetamidopropoxy group (3-A) of 3-A-AHPC contacted the same helix H12 residues and that the 3-A acetamido group was oriented toward the helix H11 arginine-396 (see Figure 3B). In addition to producing the same contacts as those of AHPN (shown in Figure 3A), the greatly accentuated twist in the diaryl bond of 3-A-AHPC produced nonplanar configurations in which the orientations of its 1-Ad group permitted close contacts with residues near and on helix H12, including leucine-416 (Figure 3E).

In Figure 3F are shown portions of the dynamics trajectory analyses of solvated RARγ LBD complexes with AHPC (**11**) and 3-A-AHPC (**10**), in which periodic boundary conditions and particle-mesh Ewald summations of electrostatic interactions were employed to provide realistic boundary forces, the damping of surface fluctuations, and the elimination of electrostatic potential truncation artifacts. These simulations having a realistic boundary force, which provided fluctuation damping at the surface of the protein, revealed that the 3-A group of 3-A-AHPC caused larger local fluctuations in residues proximate to helix H12 than the 3-chloro group of 3-Cl-AHPC did on the basis the 1-Ad C−leucine-416(CD2) C distances over time (Figure 3, panels E and F). These results were clearly analogous to those shown for AHPN (**1**) and 5-Cl-AHPN (**2**) in Figure 3C. While the compact shape of AHPC allowed intimate contacts between AHPC and residues 411−416 on helix H12, the twisted shape of 3-A-AHPC produced perturbations in local dynamics on short subnanosecond time scales that were significant enough to cause the transient opening of the LBP to the LBD surface to allow the entry of "bulk" water. The greater fluctuations evident in the distance plot for 3-A-AHPC shown in Figure 3F and the finding that LBP opening to the surface enabled bulk water entry suggested that the 3-A group had perturbed local dynamics.

Biological Results

The binding of 3-Cl-AHPC (**9**) to the RAR subtypes and RXRα was determined in competition radioligand-binding experiments using the recombinant receptor subtype LBDs and their panagonist ligand [^{3}H]9-*cis*-RA.

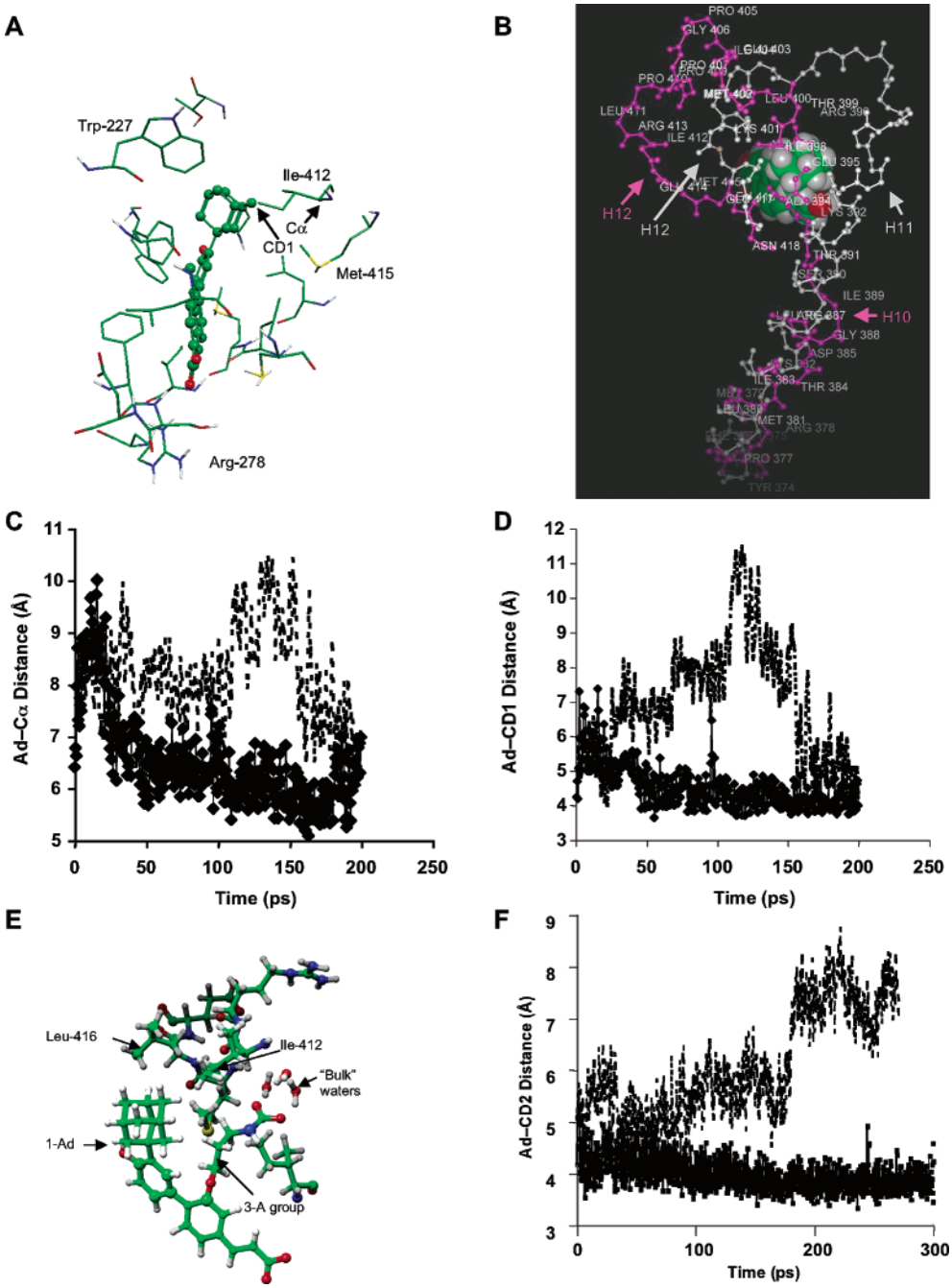

Figure 3. A substituent ortho to AHPN inter-ring bond affects time-dependent contacts between the 3′-(1-Ad) group and RARγ LBD helix H12. A. Energy-based docking of 5-Cl-AHPN (**2**) in the RARγ LBD. The lowest energy-based docked 5-Cl-AHPN orientation (shown in ball-and-stick format without Hs) and residue contacts in the RARγ LBP pocket are shown. The RARγ LBD−9-*cis*-RA (**5**) 3LBD crystal structure[65] was used for docking. The contacts of the 1-Ad group, including those with the isoleucine (Ile)-412 CD1 carbon of helix H12, are shown. Atom colorations are as in Figure 2A and S is in yellow; only Hs on side-chain heteroatoms are depicted. B. AHPN (**1**) and 5-Cl-AHPN have differential effects on the local RARγ LBD backbone conformation. The 300-ps time-points of MD simulations of AHPN (white) and 5-Cl-AHPN (magenta) in the RARγ LBD were superposed. To highlight differences, only the backbone atoms of RARγ LBD residues 371−418 and 5-Cl-AHPN are shown. The 3′-(1-Ad) and 4′-OH groups of 5-Cl-AHPN are viewed head-on. AHPN with the exception of the 3′-(1-Ad)-4′-OH-phenyl group had the same configuration as 5-Cl-AHPN in the LBP. The conformations of helix H10 (375−392) are similar, whereas those for helices H11 (393−403) and H12 (410−415) that are proximate to the 1-adamantyl (1-Ad) contacts are perturbed in the RARγ LBP−5-Cl-AHPN complex (magenta arrows) compared to the AHPN-bound conformation (gray arrows). C and D. Time dependence of the distance between the helix H12 isoleucine (Ile)-412 backbone Cα (C) or the side-chain CD1 (D) carbon (labeled in panel A) and the 1-Ad carbons of AHPN (solid line) and 5-Cl-AHPN (dashed line) in simulations of AHPN and 5-Cl-AHPN bound to the RARγ LBD are depicted graphically. E. Docking demonstrates 3-A-AHPC (**10**)−RARγ LBD helix H12 contacts. As a result of the larger diaryl bond dihedral angle, the 3-A side-chain and the 1-Ad group of 3-A-AHPC contact Ile-412 and leucine (Leu)-416, respectively. Both amino acid residues and 3-A-AHPC are represented in matchstick format with hydrogens shown in gray and other atom colorations as in Figure 2A. F. Results of molecular dynamics on AHPC (**11**) and 3-A-AHPC bound to the RARγ LBD. Time dependence of the distance between the helix H12 Leu-416 side-chain CD2 carbon and the 1-Ad carbons of AHPC (solid line) and 3-A-AHPC (dashed line). In contrast to the small fluctuations caused by close contacts between the AHPC 1-Ad and the Leu-316 CD2 carbons, large structural fluctuations resulted from the contacts between the 3-A-AHPC 1-Ad and Leu-316 CD2 carbon atoms.

Compared to nonlabeled 9-*cis*-RA (**5**), 3-Cl-AHPC (both at 1.0×10^{-6} M) only marginally displaced [^{3}H]9-*cis*-RA bound to RARα, RARβ, and RXRα (31%, 17%, and 16% displacement, respectively; Figure 4A), but quite effectively displaced [^{3}H]9-*cis*-RA bound to RARγ (83% displacement; Figure 4A). These results suggested that 3-Cl-AHPC efficiently and selectively competed with [^{3}H]9-*cis*-RA for binding to RARγ.

The binding of a coactivator protein to its site on the surface of a nuclear receptor permits the recruitment of the multiprotein complex that initiates gene transcription. X-ray crystallographic studies demonstrated that on binding a ligand capable of inducing transcriptional activation, the RARγ LBD underwent an appreciable conformational change so that its helix H12 moved from an extended conformation to one that formed the coactivator binding site with helices H3 and H4 on the LBD surface.[65] Thus, an RARγ agonist induced a change in the apo-RARγ LBD conformation to one that was more compact and protease-resistant, which was detectable by using the differential protease sensitivity assay (DPSA) coupled with mass spectral identification of the peptide fragments resulting from limited proteolysis.[70] The ability of 3-Cl-AHPC (**9**) to induce a conformational change in the [^{35}S]methionine-labeled RARγ ([^{35}S]RARγ) LBD that was indicative of agonist activity was evaluated by DPSA to determine if the peptide fragments produced would be the same as those from the LBD bound by the agonist 9-*cis*-RA (**5**). Incubation of the LBD with 9-*cis*-RA (1.0×10^{-6} M) followed by partial tryptic digestion produced two protease-resistant fragments, PF30 and PF31 (compare Figure 4B lanes 2−6 showing the proteolysis profile of the apo-RARγ LBD with lanes 12−16 showing that of the holo-LBD−9-*cis*-RA complex). PF30 and PF31 corresponded to the RARγ LBD Glu^{173}−Lys^{451} and Glu^{170}−Lys^{451} sequences, respectively.[70] 3-Cl-AHPC (5.0×10^{-6} M) also induced the formation of PF30 and PF31 (compare Figure 4B lanes 2−6 with lanes 7−11 showing the proteolytic profile of the holo-LBD−3-Cl-AHPC complex). Interestingly, the fragments induced by 3-Cl-AHPC binding appeared to be somewhat less stable to proteolytic digestion than the fragments induced by the binding of 9-*cis*-RA (compare lanes 10 and 11 with lanes 15 and 16). Nonetheless, the 3-Cl-AHPC-bound [^{35}S]RARγ LBD was clearly more resistant to tryptic digestion than the apo-[^{35}S]RARγ. Thus, the results of the DPSA studies suggested that binding by 3-Cl-AHPC and 9-*cis*-RA induced grossly similar conformational changes within the LDB of RARγ.

The RARγ comformational change that occurred on binding by a retinoid agonist was found to lead to the dissociation of an apo-receptor-associated corepressor protein such as NCoR, followed by the recruitment of a transcriptional coactivator protein such as p300.[70] Therefore, corepressor dissociation and coactivator recruitment studies were conducted to determine whether binding by 3-Cl-AHPC (**9**) promoted and/or stabilized a RARγ conformation that disfavored corepressor binding but favored coactivator binding in a manner similar to that of the classical RAR transcriptional agonists such as TTAB (**21**).[71] Both corepressor (NCoR 2110−2453) and coactivator (p300 1−450) proteins were expressed as glutathione *S*-transferase (GST) fusions in bacteria, purified, and used as affinity matrixes for the binding of the [^{35}S]RARγ LBD in standard GST-pulldown experiments, as we previously described.[70] TTAB strongly

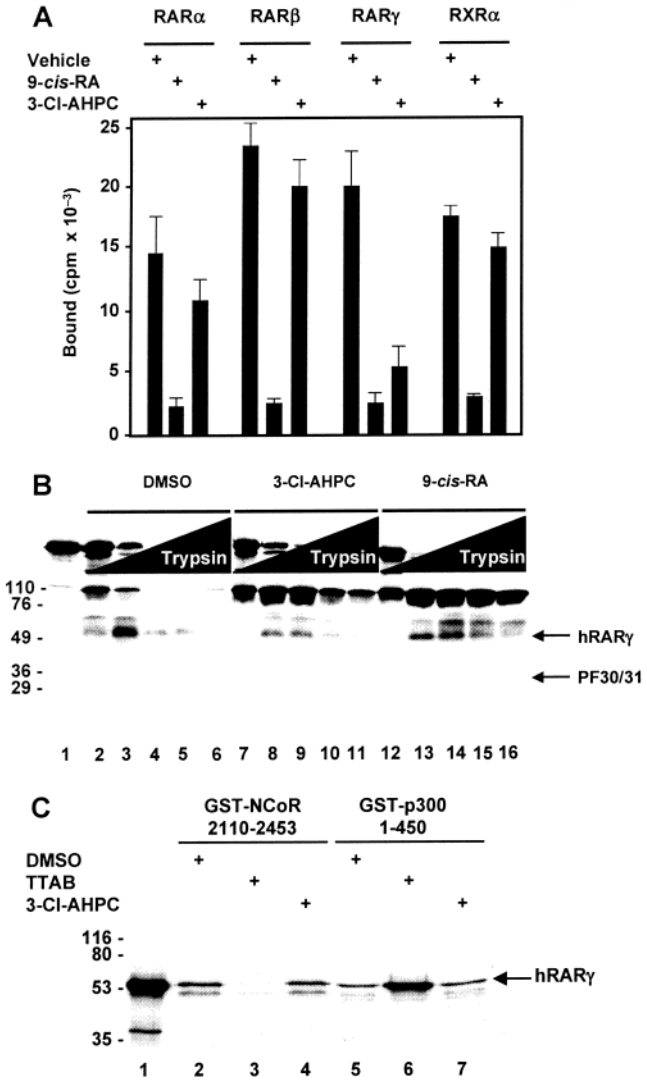

Figure 4. 3-Cl-AHPC (**9**) lacks RARγ agonist activity in vitro. A. Competition radioligand-binding experiments. Recombinant, bacterially expressed RAR subtype and RXRα LBDs (approximately 1.0×10^{-8} M) were incubated with 1.0×10^{-9} M [11,12-^{3}H$_2$]9-*cis*-RA (43 Ci/mmol) with or without 1.0×10^{-9} M nonlabeled 9-*cis*-RA (**5**) or 3-Cl-AHPC as indicated. Bound and free radioligand were separated by gel filtration using Sephadex G-50. B. 3-Cl-AHPC-bound [^{35}S]RARγ LBD is less susceptible to protolytic degradation than the *apo*-LBD. DPSAs were conducted using [^{35}S]RARγ LBD preincubated with either vehicle (DMSO, 0.1% v/v), 9-*cis*-RA (1.0×10^{-6} M), or 3-Cl-AHPC (5.0×10^{-6} M) as indicated. The receptor was then digested with increasing concentrations of trypsin-TPCK (10, 100, 250, 500, and 1000 μg/mL) for 15 min at 22 °C. Trypsin was inactivated, and the digest was subjected to electrophoresis on a denaturing gel and autoradiography. C. 3-Cl-AHPC-induced conformational change is not sufficient to induce either the dissociation of corepressor from or the recruitment of coactivator to the [^{35}S]RARγ LBD. GST-pulldown experiments were conducted using [^{35}S]RARγ LBD and either GST-NCoR 2110−2453 or GST-p300 1−450 as indicated in the presence of Me_2SO (0.1% v/v), TTAB (**21**) (1.0×10^{-6} M), or 3-Cl-AHPC (5.0×10^{-6} M) as indicated. [^{35}S]RARγ bound to GST-fusion proteins was visualized by gel electrophoresis and autoradiography. The radioligand binding data shown in A represents the mean ± SEM of three independent experiments. The autoradiographs shown in B and C are representative of three and four independent experiments, respectively.

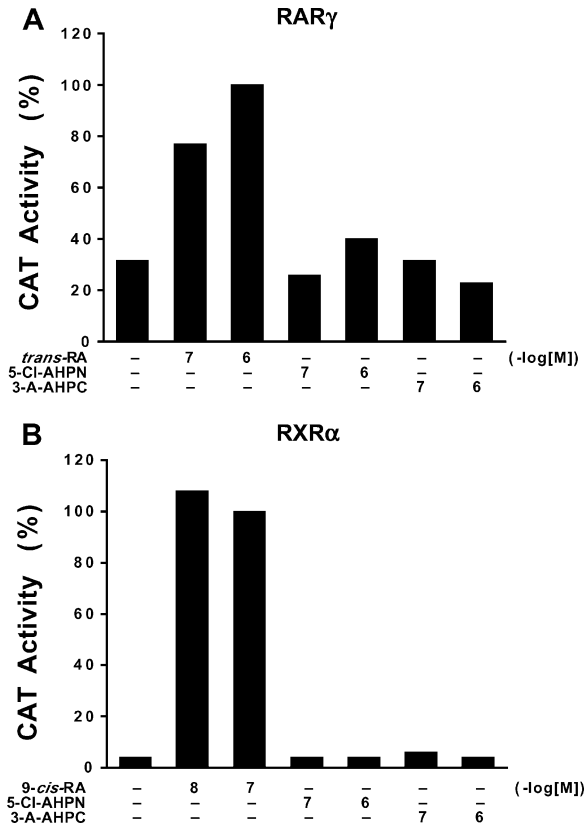

Figure 5. Transcriptional activation of RARγ by 5-Cl-AHPN (**2**) and 3-A-AHPC (**10**) compared to *trans*-RA (**4**) and that of RXRα compared to 9-*cis*-RA (**5**) on the $(TREpal)_2$-*tk*-CAT reporter in transfected CV-1 cells. Cells were treated with 1.0×10^{-7} M or 1.0×10^{-6} M 5-Cl-AHPC, 3-A-AHPC or *trans*-RA; or 1.0×10^{-8} M or 1.0×10^{-7} M 9-*cis*-RA. Reporter gene activity was normalized to that of cotransfected β-galactosidase gene activity and expressed relative to that of 1.0×10^{-6} M *trans*-RA on RARγ or 1.0×10^{-7} M 9-*cis*-RA on RXRα as 100% as described in Methods. See Experimental Section for methodology.

induced both the dissociation of GST-NCoR from [^{35}S]RARγ (compare lanes 1 and 2 in Figure 4C) and the binding of GST-p300 to [^{35}S]RARγ (compare lanes 5 and 6). In sharp contrast, 3-Cl-AHPC neither induced the dissociation of GST-NCoR from the [^{35}S]RARγ LBD (compare lanes 1 and 3) nor the binding of GST-p300 to [^{35}S]RARγ (compare lanes 5 and 7). These findings indicate that, although 3-Cl-AHPC bound to RARγ and enhanced its proteolytic stability, the type of RARγ LBD conformational change caused by 3-Cl-AHPC was not sufficient to induce either NCoR dissociation or p300 recruitment. In this respect, the behavioral profile of 3-Cl-AHPC resembled that observed for 2-(5′,6′,7′,8′-tetrahydro-5′,5′,8′,8′-tetramethyl-2′-naphthalenyl)-2-(6′-carboxy-2′-naphthalenyl)-1,3-dithiolane (**22**), which we previously characterized as an RARγ-selective retinoid that effectively antagonized the transactivation of RARγ by such agonists as *trans*-RA (**4**).[70] Subsequently, we found that the lack of RAR transcriptional agonist activity in 3-Cl-AHPC was supported by the results of reporter assays in CV-1 cells transfected with the $(TREpal)_2$-*tk*-CAT construct and a vector for RARα, β, or γ or RXRα. 3-Cl-APHC at 1.0×10^{-7} M and 1.0×10^{-6} M was transcriptionally inactive (data not shown). Similarly, both 5-Cl-AHPN (**2**) and 3-A-AHPC (**10**) at the same concentrations were unable to effectively

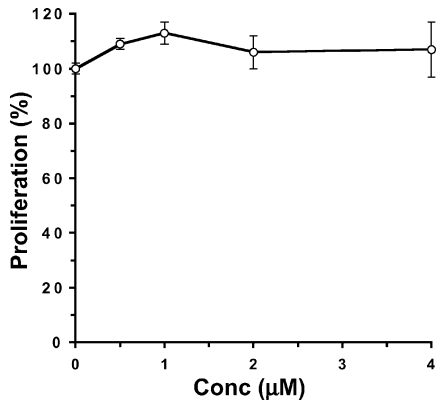

Figure 6. 3-A-AHPC (**10**) does not block 3-Cl-AHPC (**9**)-mediated inhibition of MDA-MB-468 breast cancer cell proliferation. Cells (1.0×10^6) were incubated for 24 h before the indicated concentrations of 3-A-AHPC were added. After 2 h, 0.5×10^{-6} M 3-Cl-AHPC was added, and incubation was continued for 72 h. Cells were then harvested, and proliferation in the presence of 3-A-AHPC and 3-Cl-AHPC was assessed using a colorimetric assay (see Experimental Section) and expressed relative to that of the 3-Cl-AHPC alone-treated control.

activate RARγ and RXRα (Figure 5 panels A and B, respectively).

As cancers progress to more aggressive phenotypes, the regulatory controls that hormones and retinoids exert on their proliferation can be lost. For example, unlike the MCF-7 breast cancer cell line, the growth of MDA-MB-231 and MDA-MB-468 breast cancer cell lines is neither regulated by estrogen[72] nor inhibited by standard retinoids.[2,34] Thus, the latter two cancer cell lines represent more aggressive tumors and have been used to evaluate compounds for apoptotic activity that would not be mediated by retinoid-signaling pathways. In addition, both cell lines lack functional p53,[2,72] a tumor suppressor protein involved in regulating the G_1-checkpoint of the cell cycle. p53 has been found to induce cell-cycle arrest in part through its induction of the expression of cell-cycle inhibitor $p21^{WAF1/CIP1}$, thereby permitting a cell to undergo repair in response to a stress event or to commit apoptosis. The induction of $p21^{WAF1/CIP1}$ that is independent of p53 status[73] is therapeutically advantageous because in approximately 50% of tumor samples, including those from breast cancer patients, p53 is absent or present as a nonfunctional mutant.[72,74,75] In the MDA-MB-231 and MDA-MB-468 breast cancer cell lines, AHPN (**1**)[2] and 3-Cl-AHPC (**9**) were found to induce cell-cycle arrest in G_0/G_1 through their posttranscriptional stabilization of $p21^{WAF1/CIP1}$ message and protein,[3] followed by apoptosis.[2,3]

In both breast cancer cell lines, the antagonist 3-A-AHPC (**10**) alone had no effects on cell-cycle arrest and apoptosis induction, whereas both processes were readily induced by AHPN (**1**) and its apoptotic analogues such as 5-Cl-AHPN (**2**) and 3-Cl-AHPC (**9**). Even at a concentration as high as 4.0×10^{-6} M, 3-A-AHPC after 48 or 72 h had only a minimal effect on the MDA-MB-468 cell cycle as determined by counting cell numbers (data not shown). Moreover, 3-A-AHPC at an 8-fold higher concentration was not able to block the ability of 0.5×10^{-6} M 3-Cl-AHPC to inhibit MDA-MB-468 cell proliferation (Figure 6), as evidenced by its inability to

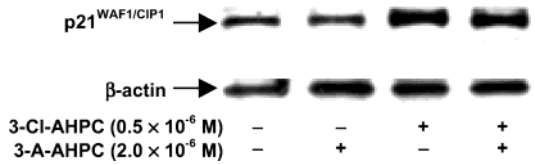

Figure 7. 3-A-AHPC (**10**) does not block the induction of $p21^{WAF1/CIP1}$ by 3-Cl-AHPC (**9**) in MDA-MB-468 breast cancer cells. Cells were grown in the presence or absence of 0.5×10^{-6} M 3-Cl-AHPC or 2.0×10^{-6} M 3-A-AHPC for 72 h, then harvested. Western blots using anti-$p21^{WAF1/CIP1}$ antibody were performed[3] (see experimental methods). β-Actin was used as the loading control.

halt cell-cycle arrest. Next, we examined the effect of 3-A-AHPC on the abilities of AHPN and 3-Cl-AHPC to induce the expression of $p21^{WAF1/CIP1}$ protein in MDA-MB-468 cells (Figure 7). Alone, 3-A-AHPC had no detectable effect on $p21^{WAF1/CIP1}$ protein levels and did not block the induction of $p21^{WAF1/CIP1}$ by 3-Cl-AHPC (Figure 7). However, 3-A-AHPC markedly inhibited MDA-MB-468 cell apoptosis induced by 3-Cl-AHPC or AHPN (Figure 8A). Antagonist 3-A-AHPC also inhibited apoptosis induced by AHPN in retinoid-resistant HL-60R leukemia cells (Figure 8B) and MDA-MB-231 breast cancer cells (Figure 8C). Even after 72 h, 3-A-AHPC alone had no apoptotic activity in HL-60R cells and had only about 6% of the apoptotic activity of AHPN against MDA-MB-231 cells, a level which we have found was within background limits in these cells. These results substantiate our earlier findings that AHPN and its analogues function through two signaling pathways in cancer cells—cell-cycle arrest and apoptosis,[2,10,73,76,77] of which only apoptosis is inhibited by the antagonist 3-A-AHPC.

We also evaluated the effects of 5-Cl-AHPN (**2**), 3-Cl-AHPC (**9**), and 3-A-AHPC (**10**) on H460 lung cancer and LNCaP prostate cancer cell lines, both of which are retinoid-sensitive and express wild-type p53 (Figure 9). 5-Cl-AHPN at 1.0×10^{-6} M induced their apoptosis at 36 h, which was partially suppressed (34% to 9%, and 31% to 15%, respectively) by an equal concentration of antagonist 3-A-AHPC, as is indicated by staining for nuclear fragmentation (Figure 9A). A 5-fold excess of 3-A-AHPC was able to decrease 1.0×10^{-6} M 3-Cl-AHPC-induced apoptosis in H460 cells from 77% to 5% (Figure 9B). AHPN (**1**), 5-Cl-AHPN, and 3-Cl-AHPC at 1.0×10^{-6} M were comparably effective at inducing

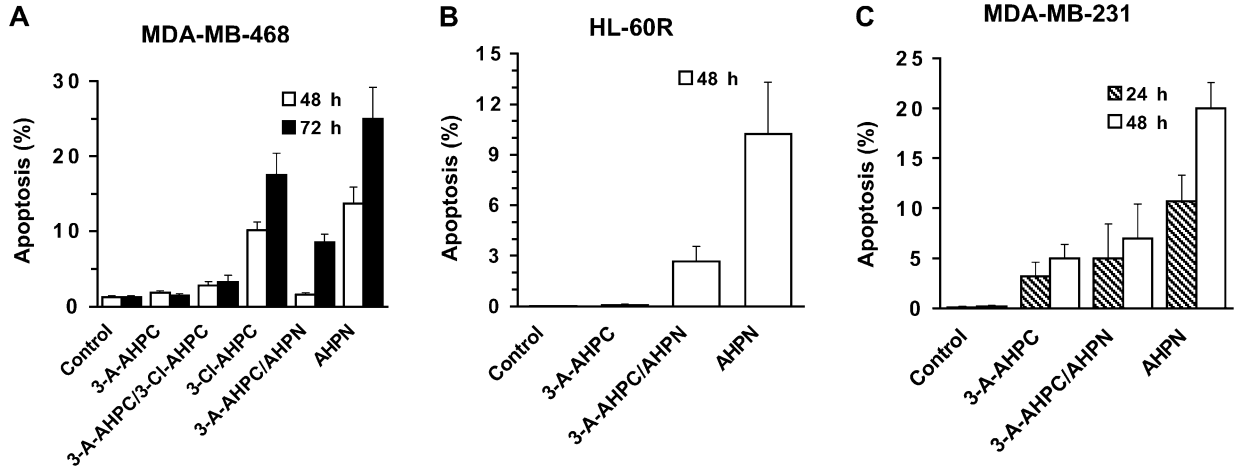

Figure 8. 3-A-AHPC (**10**) blocks 3-Cl-AHPC (**9**) and AHPN (**1**)-induced apoptosis in (A) MDA-MB-468 breast cancer, (B) HL-60R leukemia, and (C) MDA-MB-231 breast cancer cell lines. Cells were grown in the presence or absence of 0.5×10^{-6} M 3-Cl-AHPC or 0.5×10^{-6} M AHPN alone, with or without added 2.0×10^{-6} M 3-A-AHPC. Cells were harvested at 24, 48, or 72 h and acridine orange-stained.[3] Apoptotic cell numbers were determined (see methods).

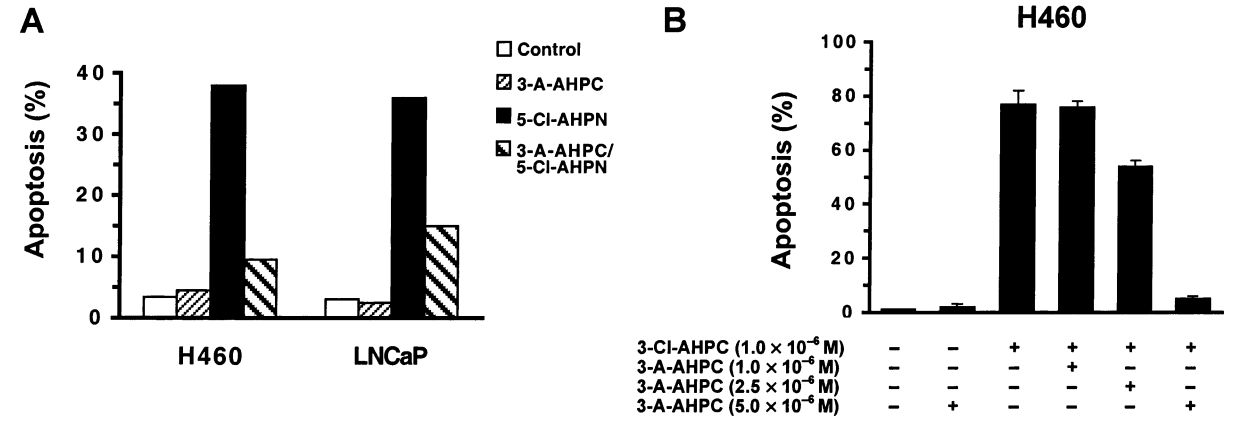

Figure 9. 3-A-AHPC (**10**) inhibits cancer cell apoptosis induced by AHPN analogues. A. H460 lung cancer and LNCaP prostate cancer cells were treated for 36 h with 1.0×10^{-6} 5-Cl-AHPN (**2**) or 1.0×10^{-6} M 3-A-AHPC alone or combined, then DAPI-stained (see methods) for visualization of nuclear morphology by fluorescence microscopy. Apoptosis levels were determined in 200-cell samples in three different fields. B. H460 cells were treated with 3-Cl-AHPC (**9**) (1.0×10^{-6} M) alone or combined with 3-A-AHPC (1.0×10^{-6} M, 2.5×10^{-6} M, or 5.0×10^{-6} M) or 3-A-AHPC (5.0×10^{-6}) alone or vehicle alone for 36 h, then DAPI-stained (see methods) and examined as in A to determine apoptosis.

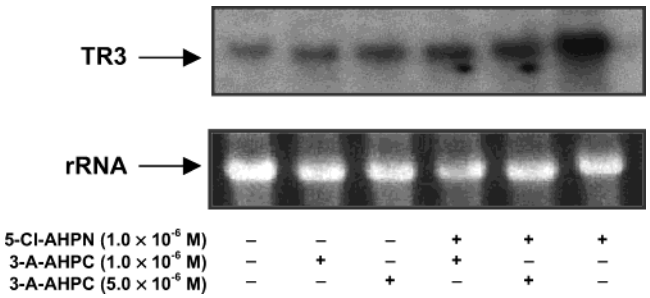

Figure 10. 3-A-AHPC (**10**) inhibits TR3 mRNA expression induced by 5-Cl-AHPN (**2**) in H460 lung cancer cells. Cells were treated for 4 h with 5-Cl-AHPN (1.0×10^{-6} M) or 3-A-AHPC (1.0×10^{-6} or 5.0×10^{-6} M) alone or combined. Total mRNAs were prepared and analyzed for TR3 expression by Northern blotting (see methods). Ethidium bromide-stained ribosomal RNA was used as the loading control.

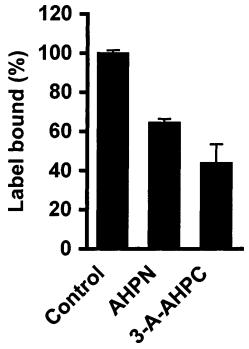

Figure 11. 3-A-AHPC (**10**) inhibits [5,5′-$^3H_2$]AHPN binding to the AHPN receptor. Nuclear extracts were prepared from HL-60R cells as we described.[4] [$^3H_2$]AHPN (1.0×10^{-8} M, 150 000 dpm) was added to the nuclear extracts in the presence or absence of nonlabeled AHPN (**1**) or 3-A-AHPC (2.0×10^{-5} M) or vehicle alone. Binding was assessed as described in the methods.

apoptosis in retinoid-resistant, p53-deficient H292 human lung cancer cells after a 40-h treatment (data not shown). Thus, the apoptotic activity found for these compounds in retinoid-refractory, p53-nonfunctional breast cancer cells extended to similarly deficient lung cancer cells, in addition to retinoid-sensitive breast, lung, and prostate cancer cells.

Earlier, we established[10] a novel pathway by which prostate and lung cancer cells underwent apoptosis induced by AHPN (**1**) and its apoptotic analogues, namely induction of the expression of the nuclear transcription factor TR3 followed by its translocation from the nucleus to the mitochondrial membrane. The association between TR3 and mitochondria was followed by mitochondrial outer membrane permeabilization and the release of mitochondrial cytochrome *c* into the cytosol,[15,78] leading to caspase activation and apoptosis.[79] As indicated in Figure 10, antagonist 3-A-AHPC (**10**) alone had no effect on the expression of TR3 mRNA in H460 cells but was able to inhibit the induction of TR3 expression by 5-Cl-AHPN (**2**).

By using binding assays and Scatchard analysis, we previously demonstrated that [5,5′-$^3H_2$]AHPN, which we had synthesized,[4] bound to a novel protein(s) contained in both HL-60R and MDA-MB-231 cell nuclear extracts.[4] Our results strongly suggested that this protein was not an RAR or RXR subtype because the RAR/RXR panagonist [10,11-$^3H_2$]9-*cis*-RA was not able to effectively compete with AHPN (**1**) for binding, and 9-*cis*-RA (**5**) did not effectively displace bound [5,5′-$^3H_2$]AHPN.[4] We next examined whether 3-A-AHPC (**10**) could inhibit the binding of [5,5′-$^3H_2$]AHPN to HL-60R nuclear extracts. As shown in Figure 11, 3-A-AHPC had efficacy similar to that shown by AHPN in displacing the tritiated label. Similar results were observed using 3-Cl-AHPC (**9**) (data not shown). Thus, 3-A-AHPC is capable of interacting with the same protein as apoptotic AHPN and 3-Cl-AHPC.

Discussion

While the configurations derived from dynamics in model simulations of AHPN (**1**) and 5-Cl-AHPN (**2**) docked in the RARγ LBP[65] could not be characterized as "holo" (bound) or "apo" (nonbound) in character, they did suggest to us that dramatic differences in local dynamics affected the recognition of a coactivator or corepressor protein by the receptor−ligand complex. Our computational results also suggested that small changes in the nature of substituents ortho to the diaryl bond in AHPN and its analogues impacted the positions of their 1-Ad groups relative to their polar termini (Figure 2A). Thus, in contrast to hydrogen and methyl groups, chloro groups significantly affected the inter-aromatic ring torsional potential surfaces so that they, in turn, altered the positions and dynamics of the 3′-(1-Ad) groups. In contrast, the carboxylate groups in these compounds remained anchored to the RARγ LBD helix H5 arginine-278.

DFT energy-minimized configurations of AHPN (**1**), 5-Cl-AHPN (**2**), 3-Cl-AHPC (**9**), 3-A-AHPC (**10**), and AHPC (**11**) are shown in Figure 2A. Our docking studies suggested that (i) 5-Cl-AHPN as initially docked was tightly packed into the LBP with close contacts to RARγ helix H12 residues; (ii) a chloro group ortho to the diaryl bond in an AHPN analogue produced a larger twist angle between the aryl rings than did an ortho hydrogen or methyl group; and (iii) the larger angle caused the 3′-(1-Ad) group to more frequently occupy positions that resulted in unfavorable interactions with the RARγ LBD helix H12. These in silico results suggested that both the position of the 3′-(1-Ad) group and the effective compound width were significantly affected by the identity of the substituent ortho to the diaryl bond on an AHPN or AHPC scaffold, which, in turn, influenced the dynamics of regions in the RAR LBD that were responsible for transcriptional response recognition.

Our experimental results supported the molecular dynamics results. Earlier, we observed that transcriptional agonist binding to the RARγ LBD produced a more compact tertiary structure that was more resistant to limited proteolytic digestion than that of the apo-receptor,[5] whereas binding by an antagonist produced a more open configuration that was more sensitive to proteolysis. The chloro group ortho to the AHPN diaryl bond reduced the ability of the AHPN analogue 3-Cl-AHPC (**9**) to interact with the RARγ LBD in terms of both its binding affinity to RARγ and the proteolytic stability of the resulting complex (Figure 4) compared to that formed by a standard retinoid agonist such as 9-*cis*-RA (**5**). Although the same peptide fragments were produced from both complexes, those from the 3-Cl-AHPC-containing complex were found to be less stable.

This result suggested that the peptides had different tertiary structures despite their originating from the cleavage of the same lysine-451 amide bond in the C-terminus of RARγ (domain F). Evidently, the subtle differences in the positions of the RARγ domain E helix H12 that occurred on binding these ligands, which were suggested by our molecular dynamics studies, did not sufficiently impact the tertiary structure of domain F so as to affect the enzymatic cleavage point but apparently made a less dramatic impact. The affinity of 3-Cl-AHPC (**9**) for the RARγ LBD was apparently lower than that of 9-*cis*-RA because a higher concentration of 3-Cl-AHPC was required to produce the same level of proteolysis obtained using 9-*cis*-RA. Moreover, 3-Cl-AHPC was not able to induce the dissociation of corepressor NCoR from the RARγ LBD or the recruitment of coactivator p300. Thus, subtle differences in the ortho substituent were able to control the degree of retinoid agonist character of the AHPNs bound in the RAR LBP, as was also evidenced by the contrasting impacts of the ortho methyl and chloro groups on RARγ transcriptional activation as reported by Dawson et al.[57] and shown in Figure 4, respectively, despite their similar sizes. Short time-scale dynamics studies (Figure 3, panels C and D) suggested that the configuration of helix H12 in RARγ bound to 5-Cl-AHPN (**2**) was less compact and produced the larger fluctuations more characteristic of those found in the apo-RARγ LBD than that of H12 in the RARγ LBD−AHPN (**1**) complex. The effect of the 3-(3′-acetamidopropoxy) group of 3-A-AHPC on the inter-ring torsion angle was even more pronounced (Figure 2, panels A and B), as was its impact on the local fluctuations of residues near and on helix H12 (Figure 3, panels E and F). Thus, these computational results provide a distinct structure−activity linkage for our substituted AHPN/AHPC analogues that may be harnessed to hamper the formation of the binding site for RAR transcriptional coactivators and minimize RAR-related toxic adverse effects while retaining apoptotic activity.

In addition to their apoptotic activity in breast cancer,[2,3,80−82] lung cancer,[5,77,83−86] and leukemia cell lines,[4,5,39,40,87−89] AHPN (**1**) and its analogues inhibited the growth and/or induced the apoptosis of other cancer cell lines, including those derived from cervical,[90] esophageal,[91] lymphoma,[92] melanoma,[93,94] neuroblastoma,[95] ovarian,[9,96−98] and prostate cancers.[10,99−101] AHPN-induced apoptosis in breast cancer cells was preceded by the expression of the cyclin kinase inhibitor p21$^{WAF1/CIP1}$ and G_0/G_1 cell-cycle arrest and was independent of the functional status of p53,[2,3] which has been found to be mutated or lost in approximately half of all tumors.[74,75] Thus, AHPN represents an important progenitor for identifying more effective agents that induce cancer cell apoptosis. This therapeutic strategy is supported by a recent finding by the Lotan group that lung cancer cells were far more sensitive to AHPN than the normal cells from which they originated[86] and our own promising in vivo findings using 3-Cl-AHPC (**9**) in a murine acute myelogenous leukemia model.[39,40]

We found that 3-A-AHPC (**10**) inhibited the induction of apoptosis by AHPN (**1**) and 3-Cl-AHPC (**9**) and the binding of both to the putative AHPN receptor in HL-60R and MDA-MB-231 nuclear extracts. The expression of TR3,[10,16,77,98] which has an essential role in the apoptosis-signaling pathway induced by AHPN analogues, was also inhibited by 3-A-AHPC. However, 3-A-AHPC did not suppress AHPN or 3-Cl-AHPC-induced p21$^{WAF1/CIP1}$ protein expression and cell-cycle arrest. These results suggest to us that the inhibition of cell proliferation, as measured by the blockade of cell-cycle progression, and the induction of apoptosis, as measured by cell morphological changes, that are induced by active members of the AHPN family represent two separate events or perhaps even separate signaling pathways. Other evidence supporting our premise of dual pathways exists in reports of cancer cell line mutants in which only one of these AHPN-sensitive pathways operates.[98,102]

The identification of an antagonist of AHPN-induced apoptosis, 3-A-AHPC (**10**), that is structurally and configurationally similar to the apoptotic analogues 5-Cl-AHPN (**2**) and 3-Cl-AHPC (**9**) strongly suggests that several earlier hypotheses on the mechanism by which AHPN initiates apoptosis may not be valid. First, because both the inducers and the inhibitor of apoptosis have similarly situated phenolic hydroxyl groups, the premise that AHPN-induced apoptosis occurs solely as the result of nonspecific free-radical generation[103,104] appears unlikely. Nonspecific mitochondrial membrane permeabilization has also been postulated as an AHPN signaling pathway.[105,106] Our findings that 3-A-AHPC blocks both 5-Cl-AHPN-induced apoptosis and TR3 expression are strong evidence that the apoptosis-initiating event probably occurs upstream of any direct effects on the mitochondrial membrane. With 3-A-AHPC available, we now have an excellent opportunity to dissect these separate AHPN-signaling pathways: (i) the 3-A-AHPC-independent suppression of cell proliferation by the induction of cell-cycle arrest; and (ii) the induction of TR3-mediated apoptosis, which is blocked by 3-A-AHPC.

Experimental Section

Chemistry. General. Starting materials were obtained from commercial sources. Unless otherwise mentioned, during workup procedures organic layers were washed with water and sat. brine, dried (anhydrous Na_2SO_4), filtered, and concentrated at reduced pressure. Standard column chromatography employed silica gel (Merck 60) as did flash chromatography (Merck, grade 9385, 230−400 mesh). Experimental procedures were not optimized and were typically conducted only twice. Melting point temperatures were determined in capillary tubes using a Mel-Temp II apparatus and are uncorrected. Fourier transform IR spectra were obtained on powdered samples, unless otherwise specified, using an FT-IR Mason satellite infrared spectrophotometer. ^{1}H NMR spectra were recorded on a 300-MHz Varian Unity Inova spectrometer unless otherwise indicated, whereas 400 MHz spectra were recorded on a Bruker instrument. Shift values are expressed in ppm (δ) relative to Me_4Si as the internal standard. Unless otherwise mentioned, spectra were run on compounds dissolved in $^2HCCl_3$. MALDI−FAB mass spectra were obtained by using an Applied Biosystems Voyager De-Pro MALDI-TOF instrument at the Institute, and MALDI−FTMS high-resolution mass spectra on an IonSpec Ultima instrument at The Scripps Research Institute (La Jolla, CA).

Ethyl 4-Bromo-3-hydroxybenzoate (25). According to a reported procedure,[107] $MeSO_3H$ (2.0 mL) was added to **23** (5.0 g, 0.036 mol) in EtOH (10 mL) and benzene (100 mL). The reaction mixture was heated at reflux (10 h, Dean−Stark trap), cooled, washed (water, 5% $NaHCO_3$, and sat. brine), dried, and

concentrated to a solid, which was chromatographed (10% EtOAc/hexane) to give ethyl ester **24** (5.65 g, 94%) as a white powder, mp 71−73 °C, which was used without further purification.

A reported procedure for 4-bromo-3-hydroxybenzoic acid[108] was modified to substantially improve the yield of **25**. To a stirred solution of **24** (332 mg, 2.0 mmol) in glacial HOAc (2.0 mL) was slowly added Br_2 (320 mg, 2 mmol) in HOAc (1.0 mL) with stirring at room temperature. After stirring for 6 h, additional Br_2 (90 mg, 0.56 mmol) in HOAc (0.3 mL) was added, and stirring was continued (14 h). Ether (50 mL) was added, and the organic layer was washed (water, 5% $NaHCO_3$, and sat. brine), dried, and concentrated to an oil. Chromatography (8% EtOAc/8% CH_2Cl_2/hexane) gave **25** as a white powder (260 mg, 53%), mp 90−92 °C. TLC (17% EtOAc/hexanes) R_f 0.47. FT-IR ($CHCl_3$) 3388, 1695, cm^{-1}. ^1H NMR δ 1.39 (t, J = 7.2 Hz, 3H, CH_3), 4.37 (q, J = 7.2 Hz, 2H, OCH_2), 5.75 (s, 1H, OH), 7.48 (d, J = 8.1 Hz, 1H, 6-ArH), 7.55 (d, J = 8.1 Hz, 1H, 5-ArH), 7.68 ppm (s, 1H, 2-ArH).

Ethyl 4-Bromo-3-benzyloxybenzoate (26). To a suspension of **25** (4.5 g, 18.4 mmol) and K_2CO_3 (4.1 g, 30 mmol) in acetone (150 mL) under Ar was added benzyl bromide (3.4 g, 20 mmol). The mixture was heated at reflux for 15 h, concentrated, then diluted with CH_2Cl_2 (100 mL), washed (water, 1 N HCl, and brine), and dried. Concentration and chromatography (5% EtOAc/hexane) afforded 5.2 g (84%) of **26** as a white powder, mp 50−52 °C. TLC (20% CH_2Cl_2/hexane) R_f 0.35. FT-IR ($CHCl_3$) 1722 cm^{-1}. ^1H NMR δ 1.39 (t, J = 7.2 Hz, 3H, CH_3), 4.37 (q, J = 7.2 Hz, 2H, OCH_2), 5.21 (s, 2H, OCH_2Ph), 7.39 (m, 3H, ArH), 7.50 (m, 3H, ArH), 7.63 ppm (m, 2H, ArH). MALDI−FTMS (HRMS) calcd $C_{16}H_{15}BrNaO_3$ [MNa^+] 357.0097, found 357.0093.

4-Bromo-3-benzyloxybenzyl Alcohol (27). To **26** (3.35 g, 10 mmol) dissolved in CH_2Cl_2 (25 mL) and cooled under Ar in a dry ice−acetone bath was slowly added 20 mL of 1.0 M DIBAL (20 mmol) in hexanes with stirring. After 2 h, the stirred reaction mixture was diluted with 1 N HCl (20 mL) and CH_2Cl_2 (50 mL), and stirring was continued for 0.5 h. The organic layer was washed and dried. Concentration and chromatography (9% EtOAc/hexane) afforded 2.78 g (91%) of **27** as a white solid, mp 73−75 °C. TLC (9% EtOAc/hexane) R_f 0.17. FT-IR (powder) 3383 cm^{-1}. ^1H NMR δ 4.63 (d, J = 5.7 Hz, 2H, $ArCH_2O$), 5.16 (s, 2H, OCH_2Ph), 6.83 (d, J = 8.1 Hz, 1H, 6-ArH), 7.00 (s, 1H, 2-ArH), 7.33−7.54 (m, 5H, ArH), 7.53 ppm (d, 1H, 5-ArH). MALDI−FTMS (HRMS) calcd $C_{14}H_{13}BrNaO_2$ [MNa^+] 314.9991, found 314.9998.

Ethyl (*E*)-4-Bromo-3-benzyloxycinnamate (29). To a stirred solution of **27** (2.77 g, 10 mmol) in CH_2Cl_2 (30 mL) cooled in an ice bath was slowly added PCC (3.23 g, 15 mmol). This mixture was stirred for 5 h at room temperature before Et_2O (50 mL) was added. Filtration and concentration gave the 3-benzyloxy-4-bromobenzaldehyde (**28**) as a white powder, which was used in the next step without further purification.

To triethyl phosphonoacetate (0.33 g, 1.5 mmol) dissolved in anhydrous Et_2O (10 mL) then cooled in a dry ice−acetone bath was added 1.5 mL of 0.91 M $KN(SiMe_3)_2$ (1.35 mmol) in THF under Ar with stirring, which was continued for 0.5 h. Next, **28** (0.24 g, 0.83 mmol) in Et_2O (10 mL) was slowly added to the solution with cooling in the dry ice−acetone bath. After stirring for 1 h more, the mixture was allowed to warm to ambient temperature, stirred overnight, poured into water (50 mL) containing HOAc (1.0 mL), and extracted into Et_2O (20 mL). The extract was washed, dried, and concentrated. Chromatography (5% EtOAc/hexane) of the residue afforded 0.28 g (91%) of **29** as a white solid, mp 45−48 °C. TLC (9% EtOAc/hexane) R_f 0.67. FT-IR ($CHCl_3$) 1711, 1640 cm^{-1}. ^1H NMR δ 1.33 (t, J = 7.2 Hz, 3H, CH_3), 4.26 (q, J = 6.9 Hz, 2H, CH_2), 5.18 (s, 2H, CH_2Ph), 6.39 (d, J = 15.9 Hz, 1H, ArCH=C), 7.01 (d, J = 8.4 Hz, 1H, 6-ArH), 7.06 (s, 1H, 2-ArH), 7.33−7.50 (m, 5H, ArH), 7.57 (d, J = 8.4 Hz, 1H, 5-ArH), 7.58 ppm (d, J = 15.9 Hz, 1H, C=$CHCO_2$). MALDI−FTMS (HRMS) calcd $C_{18}H_{18}BrO_3$ [MH^+] 361.0434, found 361.0437.

Ethyl (*E*)-4-Bromo-3-hydroxycinnamate (30). A solution of **29** (260 mg, 0.72 mmol) in CH_2Cl_2 (5 mL) and 1.0 M BBr_3 (1.5 mmol) in CH_2Cl_2 (1.5 mL) was stirred at −78 °C under Ar for 2 h, then diluted with water (10 mL) and CH_2Cl_2 (20 mL). The organic phase was washed, dried, and concentrated. Flash chromatography (10% EtOAc/hexane) gave **30** as a white powder (180 mg, 92%), mp 135−137 °C. TLC (9% EtOAc/hexanes) R_f 0.25. FT-IR ($CHCl_3$) 3328, 1678 cm^{-1}. ^1H NMR δ 1.34 (t, J = 6.9 Hz, 3H, CH_3), 4.27 (q, J = 7.2 Hz, 2H, OCH_2), 5.62 (s, 1H, OH), 6.42 (d, J = 15.9 Hz, 1H, ArCH=C), 6.98 (d, J = 8.4 Hz, 1H, 6-ArH), 7.18 (s, 1H, 2-ArH), 7.48 (d, J = 8.1 Hz, 1H, 5-ArH), 7.58 ppm (d, J = 15.9 Hz, 1H, C=$CHCO_2$). MALDI−FTMS (HRMS) calcd $C_{11}H_{12}BrO_3$ [MH^+] 270.9970, found 270.9971.

Ethyl (*E*)-4-Bromo-3-(3′-*tert*-butoxycarboxamidopropoxy)cinnamate (31). A suspension of **30** (320 mg, 1.18 mmol) and K_2CO_3 (500 mg, 3.62 mmol) in acetone (50 mL) containing 3-(*tert*-butoxycarboxamido)propyl bromide (**33**) (480 mg, 1.98 mmol) was heated at reflux under Ar for 20 h, then concentrated. The residue was extracted with CH_2Cl_2, and the extract was washed (water, 1 N HCl, and brine) and dried. Concentration and chromatography (10% EtOAc/hexane) of the residue afforded 410 mg (81%) of **31** as a white powder, mp 65−67 °C. TLC (17% EtOAc/hexane) R_f 0.30. FT-IR 3425, 2980, 1706 cm^{-1}. ^1H NMR δ 1.34 (t, J = 7.2 Hz, 3H, CH_3), 1.44 (s, 9H, $OC(CH_3)_3$), 2.07 (t, J = 6.0 Hz, 2H, 2′-CH_2), 3.40 (q, J = 5.7 Hz, 2H, 3′-CH_2N), 4.13 (t, J = 5.7 Hz, 2H, 1′-CH_2O), 4.26 (q, J = 7.2 Hz, 2H, OCH_2), 5.22 (s, 1H, NH), 6.47 (d, J = 15.9 Hz, 1H, ArCH=C), 7.00 (s, 1H, 2-ArH), 7.01 (d, J = 6.3 Hz, 1H, 6-ArH), 7.54 (d, J = 8.7 Hz, 1H, 5-ArH), 7.60 ppm (d, J = 15.9 Hz, 1H, C=$CHCO_2$). MALDI−FTMS (HRMS) calcd $C_{19}H_{26}BrNNaO_5$ [MNa^+] 450.0886, found 450.0889.

3-Bromo-1-(*tert*-butoxycarbonyl)propylamine (33). A reported procedure was applied[109] to 3-bromopropylamine hydrobromide (**32**) (4.4 g, 20 mmol), Et_3N (3.0 mL, 20 mmol), and di-(*tert*-butyl)dicarbonate (5.5 g, 25 mmol) in CH_2Cl_2 (20 mL) to give after workup and chromatography (5% EtOAc/hexane) 3.95 g (83%) of **33** as a colorless liquid. TLC (17% EtOAc/hexane) R_f 0.61. FT-IR (film) 3399, 1678 cm^{-1}. ^1H NMR δ 1.45 (s, 9H, $OC(CH_3)_3$), 2.05 (m, 2H, 2-CH_2), 3.28 (q, J = 6.3 Hz, 2H, 1-CH_2N), 3.45 (t, J = 6.3 Hz, 2H, 3-CH_2Br), 4.66 ppm (s, 1H, NH).

Ethyl (*E*)-4-[3′-(1-Adamantyl)-4′-benzyloxyphenyl]-3-[(3′-*tert*-butoxycarboxamido)propoxy]cinnamate (38). To **31** (321 mg, 0.75 mmol), 3-(1-adamantyl)-4-benzyloxyphenylboronic acid[5] (**37**) (362 mg, 1.0 mmol), and $Pd(PPh_3)_4$ (60 mg, 0.052 mmol) in DME (5 mL) was added under Ar with stirring 2.0 M aq Na_2CO_3 (1.0 mL). The reaction mixture was heated at reflux for 20 h, cooled to room temperature, then extracted (EtOAc). The extract was washed, dried, and concentrated. Flash chromatography (EtOAc/hexane) of the residue gave **38** as a yellow powder (410 mg, 83%), mp 73−75 °C, which was used without further purification in the deprotection steps to give **10** and **14**. TLC (20% EtOAc/hexane) R_f 0.30. FT-IR 3366, 1711 cm^{-1}. ^1H NMR δ 1.35 (t, J = 6.9 Hz, 3H, CH_3), 1.43 (s, 9H, $OC(CH_3)_3$), 1.72 (s, 6H, $AdCH_2$), 1.95 (m, 2H, 2′-CH_2), 2.04 (s, 3H, AdCH), 2.17 (s, 6H, $AdCH_2$), 3.24 (d, J = 5.4 Hz, 2H, 3′-CH_2N), 4.03 (t, J = 5.7 Hz, 2H, 1′-CH_2O), 4.28 (q, J = 6.6 Hz, 2H, OCH_2), 4.55 (s, 1H, NH), 5.16 (s, 2H, OCH_2Ph), 6.45 (d, J = 15.9 Hz, 1H, ArCH=C), 7.00 (d, J = 8.7 Hz, 1H, 5′-ArH), 7.11 (s, 1H, 2-ArH), 7.20 (d, J = 7.8 Hz, 1H, 6′-ArH), 7.34−7.45 (m, 5H, ArH), 7.51 (s, 1H, 2′-ArH), 7.53 (d, J = 7.2 Hz, 2H, 5,6-ArH), 7.68 ppm (d, J = 15.9 Hz, 1H, C=$CHCO_2$). MALDI−FAB calcd $C_{42}H_{52}NO_6$ [MH^+] 664.8, found 664.8.

Ethyl (*E*)-4-[3′-(1-Adamantyl)-4′-benzyloxyphenyl]-3-(3′-acetamidopropoxy)cinnamate (40). To a mixture of **38** (400 mg, 0.6 mmol) in EtOH (10 mL) was added concentrated HCl (1.0 mL). This mixture was heated at reflux for 1 h, then concentrated. The residue containing the primary amine **39** was sequentially treated with CH_2Cl_2 (20 mL), pyridine (1.0 mL), and Ac_2O (1.0 mL) and stirred overnight at room temperature before being washed, dried ($MgSO_4$), and concentrated. Flash chromatography (EtOAc/hexane) gave **40** as a white powder (280 mg, 77%), mp 80−82 °C. TLC (67% EtOAc/hexane) R_f 0.28. FT-IR 3293, 1716 cm^{-1}. ^1H NMR δ 1.35 (t, J = 7.2 Hz, 3H, CH_3), 1.45 (s, 2H, 2′-CH_2), 1.72 (s, 6H,

$AdCH_2$), 2.04 (s, 6H, AdCH and $COCH_3$), 2.15 (s, 6H, $AdCH_2$), 3.37 (q, J = 5.4 Hz, 2H, 3′-CH_2N), 4.12 (t, J = 5.1 Hz, 2H, 1′-CH_2O), 4.28 (q, J = 7.2 Hz, 2H, OCH_2), 5.15 (s, 2H, OCH_2Ph), 5.67 (s, 1H, NH), 6.45 (d, J = 16.2 Hz, 1H, ArCH=C), 7.00 (d, J = 7.8 Hz, 1H, 5′-ArH), 7.09 (s, 1H, 2′-ArH), 7.22 (d, J = 7.8 Hz, 1H, ArH), 7.26−7.42 (m, 5H, ArH), 7.45 (d, 1H, J = 6.9 Hz, 1H, ArH), 7.49 (s, 1H, 2-ArH), 7.50 (d, J = 8.1 Hz, 1H, ArH), 7.69 ppm (d, J = 16.2 Hz, 1H, C=$CHCO_2$). MALDI−FTMS (HRMS) calcd $C_{39}H_{45}NNaO_5$ (MNa^+) 630.3190, found 630.3172.

Ethyl (*E*)-4-[3′-(1-Adamantyl)-4′-hydroxyphenyl]-3-(3′-acetamidopropoxy)cinnamate (41). A solution of **40** (303 mg, 0.5 mmol) and 1.0 M BBr_3 (1.5 mmol) in CH_2Cl_2 (1.5 mL) and CH_2Cl_2 (5 mL) was stirred at −78 °C under Ar for 2 h, then diluted with water (10 mL) and CH_2Cl_2 (20 mL). The organic phase was washed, dried, and concentrated. Flash chromatography (EtOAc/hexane) gave **41** as an off-white powder (226 mg, 77%), mp 110−113 °C. TLC (67% EtOAc/hexane) R_f 0.20. FT-IR 3408, 1706, 1637 cm^{-1}. ^1H NMR δ 1.35 (t, J = 6.9 Hz, 3H, CH_3), 1.44 (s, 2H, 2′-CH_2), 1.77 (s, 6H, $AdCH_2$), 2.04 (s, 3H, AdCH). 2.08 (s, 3H, $COCH_3$), 2.14 (s, 6H, $AdCH_2$), 3.38 (q, J = 5.4 Hz, 2H, 3′-CH_2N), 4.13 (t, J = 6.3 Hz, 2H, 1′-CH_2O), 4.27 (q, J = 7.2 Hz, 2H, OCH_2), 5.81 (s, 1H, NH), 6.30 (s, 1H, OH), 6.44 (d, J = 15.9 Hz, 1H, ArCH=C), 6.75 (d, J = 8.1 Hz, 1H, 5′-ArH), 7.09 (s, 1H, 2′-ArH), 7.20 (d, J = 7.5 Hz, 1H, ArH), 7.26 (d, J = 8.1 Hz, 1H, ArH), 7.33 (d, J = 8.1 Hz, 1H, ArH), 7.40 (s, 1H, 2-ArH), 7.68 ppm (d, J = 15.9 Hz, 1H, C=$CHCO_2$). MALDI−TFMS (HRMS) calcd $C_{32}H_{40}NO_5$ (MH^+) 518.2906, found 518.2892.

(*E*)-4-[3′-(1-Adamantyl)-4′-hydroxyphenyl]-3-(3′-acetamidopropoxy)cinnamic Acid (10). To a suspension of **41** (190 mg, 0.387 mmol) in MeOH (10 mL) was added NaOH (100 mg, 2.5 mmol). The mixture was stirred at reflux temperature under Ar for 1 h, cooled to room temperature, acidified (1 N HCl), and extracted (EtOAc). The extract was washed, dried ($MgSO_4$), and concentrated to afford **10** as an off-white powder (170 mg, 94%), mp 195−199 °C. FT-IR (powder) 3400, 1691, 1632 cm^{-1}. ^1H NMR (DMSO-$^2H_6$) δ 1.73 (s, 6H, $AdCH_2$), 1.77 (s, 3H, $COCH_3$), 1.78 (m, 2H, 2′-CH_2), 2.03 (s, 3H, AdCH), 2.10 (s, 6H, $AdCH_2$), 3.17 (d, J = 5.4 Hz, 2H, 3′-CH_2N), 4.06 (broad s, 2H, 3′-CH_2O), 6.63 (d, J = 15.9 Hz, 1H, ArCH=C), 6.80 (d, J = 8.1 Hz, 1H, 5′-ArH), 7.21 (d, J = 8.7 Hz, 1H, ArH), 7.29 (s, 3H, ArH and 2′-ArH), 7.37 (s, 1H, 2-ArH), 7.61 (d, J = 15.9 Hz, 1H, C=$CHCO_2$), 7.86 (s, 1H, NH), 9.41 ppm (s, 1H, OH). MALDI−FTMS (HRMS) calcd $C_{30}H_{35}NNaO_5$ [MNa^+] 512.2407, found 512.2402.

Ethyl (*E*)-4-[3′-(1-Adamantyl)-4′-hydroxyphenyl]-3-(3′-aminopropoxy)cinnamate (43). A solution of **38** (500 mg, 0.75 mmol) and 1.0 M BBr_3 (1.5 mmol) in CH_2Cl_2 (1.5 mL) and CH_2Cl_2 (20 mL) was stirred at −78 °C under Ar for 2 h, then diluted with water (10 mL) and CH_2Cl_2 (20 mL). The organic phase was washed, dried, and concentrated to give ethyl (*E*)-4-[3′-(1-adamantyl)-4′-hydroxyphenyl]-3-(3′-*tert*-butoxycarboxamido)propoxycinnamate (**42**) as a pale-yellow solid. The solid in EtOH (20 mL) containing concentrated HCl (1.5 mL) was heated at reflux under Ar for 2 h. The solution was concentrated before dilution with MeOH (20 mL). $NaHCO_3$ (200 mg) was added, and this mixture was stirred for 1 h under Ar, then concentrated. Flash chromatography (9% MeOH/CH_2Cl_2) gave **43** as a white solid (278 mg, 78%), mp 181−183 °C. TLC (9% MeOH/CH_2Cl_2) R_f 0.62. FT-IR 3244, 1706, 1632 cm^{-1}. ^1H NMR δ 1.34 (t, J = 7.2 Hz, 3H, CH_3), 1.76 (s, 6H, $AdCH_2$), 1.94 (m, 2H, 2′-CH_2), 2.05 (s, 3H, AdCH), 2.15 (s, 6H, $AdCH_2$), 2.85 (m, 2H, 3′-CH_2N), 3.74 (s, 2H, NH_2), 4.09 (s, 2H, 3′-CH_2O), 4.28 (q, J = 7.5 Hz, 2H, OCH_2), 5.71 (s, 1H, OH), 6.43 (d, J = 15.9 Hz, 1H, ArCH=C), 6.62 (d, J = 7.8 Hz, 1H, 5′-ArH), 7.08 (s, 1H, 2-ArH), 7.17 (d, J = 7.2 Hz, 1H, ArH), 7.20 (d, J = 8.4 Hz, 1H, ArH), 7.30 (s, 1H, 2′-ArH), 7.32 (d, J = 7.5 Hz, 1H, ArH), 7.68 ppm (d, J = 15.9 Hz, 1H, C=$CHCO_2$). MALDI−FTMS (HRMS) calcd $C_{30}H_{38}NO_4$ [MH^+] 476.2795, found 476.2790.

(*E*)-4-[3′-(1-Adamantyl)-4′-hydroxyphenyl]-3-(3′-aminopropoxy)cinnamic Acid (14). To a suspension of **43** (260 mg, 0.547 mmol) in MeOH (10 mL) was added NaOH (100 mg, 2.5 mmol) in water (1.0 mL). The reaction mixture was stirred at reflux temperature under Ar for 1 h, cooled to room temperature, acidified (1 N HCl), and concentrated. The resultant solid was diluted with water (5 mL) and Et_2O (10 mL), then stirred for 1 h, filtered, and dried under vacuum to give **14** as an off-white powder (236 mg, 89%), mp 238−240 °C. FT-IR 3381, 1686 cm^{-1}. ^1H NMR (CD_3OD) δ 1.87 (s, 6H, $AdCH_2$), 2.11 (s, 3H, AdCH), 2.13 (m, 2H, 2′-CH_2), 2.24 (s, 6H, $AdCH_2$), 3.08 (t, J = 7.5 Hz, 2H, 3′-CH_2N), 4.20 (t, J = 6.0 Hz, 2H, 1′-CH_2O), 6.56 (d, J = 16.2 Hz, 1H, ArCH=C), 6.81 (d, J = 8.4 Hz, 1H, 5′-ArH), 7.23 (d, J = 8.4 Hz, 1H, 6′-ArH), 7.30 (d, J = 8.4 Hz, 2H, ArH), 7.33 (s, 2H, 2,2′-ArH), 7.73 ppm (d, J = 16.2 Hz, 1H, C=$CHCO_2$). MALDI−FTMS (HRMS) calcd $C_{28}H_{34}NO_4$ (MH^+) 448.2482, found 448.2488.

Ethyl 5-Chloro-6-hydroxy-2-naphthalenecarboxylate (46). A suspension of **44** (4.90 g, 26.0 mmol), in EtOH (25 mL) was treated with concentrated H_2SO_4 (1.0 g), stirred for 5 days, then heated at reflux for 1 h to complete esterification. After removal of EtOH at reduced pressure, the ethyl ester **45** was isolated by extraction (EtOAc), followed by washing (2 × 5% $NaHCO_3$ and sat. brine) and drying ($MgSO_4$). Concentration and crystallization afforded **45** (4.81 g, 85%), mp 109−110 °C. TLC (EtOAc) R_f 0.83. ^1H NMR (400 MHz) δ 1.47 (t, J = 7.0 Hz, 3H, CH_3), 4.47 (q, J = 7.0 Hz, 2H, CH_2), 6.13 (s, 1H, OH), 7.19 (dd, J = 8.8 Hz, J = 2.4 Hz, 1H, 7-NapH), 7.20 (s, 1H, 5-NapH), 7.70 (d, J = 8.5 Hz, 1H, 8-NapH), 7.87 (d, J = 8.3 Hz, 1H, 4-NapH), 8.01 (dd, J = 8.6 Hz, J = 1.8 Hz, 1H, 3-NapH), 8.54 ppm (d, J = 0.8 Hz, 1H, 1-NapH). Anal. ($C_{13}H_{12}O_3$) C, H. MALDI−FTMS (HRMS) calcd $C_{13}H_{13}O_3$ (MH^+) 217.0859, found 217.0861.

α-Chlorination of **45** was conducted by modifying a reported procedure.[59] To a solution of **45** (3.62 g, 16.7 mmol) in glacial HOAc (32 mL) was added sulfuryl chloride (2.27 g, 16.8 mmol). The mixture heated for 2.5 h at 70 °C, then stirred at room temperature for 36 h. Concentration, ice-bath cooling, and filtration afforded **46** as white crystals (2.60 g, 62%), mp 139−142 °C. TLC (20% EtOAc/benzene) R_f 0.61. ^1H NMR (400 MHz) δ 1.45 (t, J = 5.4 Hz, 3H, CH_3), 4.44 (q, J = 5.4 Hz, 2H, CH_2), 6.16 (s, 1H, OH), 7.32 (d, J = 8.8 Hz, 1H, 7-NapH), 7.82 (d, J = 8.8 Hz, 1H, 8-NapH), 8.07 (d, J = 8.8 Hz, 1H, 4-NapH), 8.15 (dd, J = 8.8 Hz, J = 1.6 Hz, 1H, 3-NapH), 8.54 ppm (s, 1H, 1-NapH). Anal. ($C_{13}H_{11}ClO_3$) C, H. MALDI−FTMS (HRMS) calcd $C_{13}H_{12}ClO_3$ (MH^+) 251.0469, found 251.0473.

Ethyl 6-[3′-(1-Adamantyl)-4′-benzyloxyphenyl]-5-chloro-2-naphthalenecarboxylate (48). To **46** (2.05 g, 8.18 mmol) and pyridine (2.0 mL, 25 mmol) dissolved in CH_2Cl_2 (55 mL) and cooled in an ice bath was added over a 5-min period trifluoromethanesulfonic anhydride (1.7 mL, 10.1 mmol). The reaction mixture was allowed to warm to room temperature, stirred for 18 h, washed (2 × H_2O, 10% HCl, and sat. brine), then dried ($MgSO_4$). Concentration afforded ethyl 5-chloro-6-trifluoromethanesulfonyloxy-2-naphthalenecarboxylate (**47**) as white crystals (2.43 g, 78%), mp 99−100 °C. TLC (25% EtOAc/hexane) R_f 0.80, which was used without further purification in the following step. ^1H NMR δ 1.47 (t, J = 6.9 Hz, 3H, CH_3), 4.47 (d, J = 6.8 Hz, 2H, CH_2), 7.52 (d, J = 8.9 Hz, 1H, 7-NapH), 7.97 (d, J = 9.0 Hz, 1H, 8-NapH), 8.27 (d, J = 8.7 Hz, 1H, 4-NapH), 8.37 (d, J = 8.8 Hz, 1H, 3-NapH), 8.64 ppm (s, 1H, 1-NapH).

To a solution of arylboronic acid **37** (500 mg, 1.38 mmol), triflate **47** (524 mg, 1.37 mmol), $Pd(PPh_3)_4$ (165 mg, 0.143 mmol), and LiCl (114 mg, 2.69 mmol) in dimethoxyethane (12 mL) under Ar was added 2.0 M aq Na_2CO_3 (1.4 mL). The reaction mixture was heated at reflux (18 h), diluted (EtOAc and sat. brine), and extracted (CH_2Cl_2). The organic extract was dried ($MgSO_4$) and concentrated. Flash chromatography (5% EtOAc/hexane) of the residue and concentration provided **48** as white crystals (420 mg, 56%), mp 177−179 °C. TLC (10% EtOAc/hexane) R_f 0.37. FT-IR (KBr) 1716 cm^{-1}. ^1H NMR (400 MHz) δ 1.47 (t, J = 6.0 Hz, 3H, CH_3), 1.74 (s, 6, $AdCH_2$), 2.05 (s, 3H, AdH), 2.20 (s, 6H, $AdCH_2$), 4.46 (q, J = 7.0 Hz, 2H, OCH_2), 5.20 (s, 2, $CHPh_2$), 7.06 (d, J = 8.8 Hz, 1H, 5-ArH), 7.3−7.4 (m, 2, ArH), 7.4−7.5 (m, 3, ArH), 7.5−7.6 (m, 3, ArH and 7-NapH), 7.90 (d, J = 8.0 Hz, 1H, 8-NapH), 8.20 (dd, J =

8.8 Hz, J = 1.6 Hz, 1H, 3-NapH), 8.44 (d, J = 8.8 Hz, 1H, 4-NapH), 8.62 ppm (d, J = 1.6 Hz, 1H, 1-NapH). MALDI−FTMS (HRMS) calcd $C_{36}H_{36}ClO_2$ (MH^+) 550.2275, found 550.2285.

Ethyl 6-[3′-(1-Adamantyl)-4′-hydroxyphenyl]-5-chloro-2-naphthalenecarboxylate (49). To **48** (170 mg, 0.31 mmol) dissolved in CH_2Cl_2 (30 mL) and cooled in a dry ice−EtOH bath was added 1.0 M BBr_3 (900 mmol) in CH_2Cl_2 (0.90 mL) over a 2-min period. After being stirred at this temperature for 1 h, the mixture was diluted with cold H_2O (10 mL) and allowed to warm to room temperature. The organic layer was separated, dried ($MgSO_4$), and concentrated to give **49** as white crystals (101 mg, 71%), mp 256−260 °C. TLC (toluene) R_f 0.26. ^{1}H NMR (300 MHz, $CDCl_3$) δ 1.47 (t, J = 7.0 Hz, 3H, CH_3), 1.80 (s, 6H, $AdCH_2$), 2.10 (s, 3H, AdCH), 2.18 (s, 6H, $AdCH_2$), 4.47 (q, J = 7 Hz, 2H, CH_2), 4.91 (s, 1H, OH), 5.30 (s, 2H, CH_2), 6.77 (d, J = 7.3 Hz, 1H, 5′-ArH), 7.38 (s, 1H, 2′-ArH), 7.54 (d, J = 8.1 Hz, 2H, 7-NapH and 6′-ArH), 7.90 (d, J = 9.6 Hz, 1H, 8-NapH), 8.19 (d, J = 9.0 Hz, 1H, 4-NapH), 8.44 (d, J = 9.0 Hz, 1H, 3-NapH), 8.62 ppm (s, 1H, 1-NapH). MALDI−FTMS (HRMS) calcd $C_{29}H_{30}ClO_2$ (MH^+) 460.1805, found 460.1798.

6-[3′-(1-Adamantyl)-4′-hydroxyphenyl]-5-chloro-2-naphthalenecarboxylic Acid (2). A suspension of **49** (230 mg, 0.50 mmol) in 1.0 M NaOH in 75% aq EtOH (5 mL) was heated at reflux for 40 min, cooled, acidified (10% HCl), then extracted (EtOAc). The extract was washed (sat. brine), dried ($MgSO_4$), and concentrated to give **2** as a white powder (205 mg, 95%), mp 282−284 °C (dec). TLC (5% MeOH/$CHCl_3$) R_f 0.26. FT-IR 2983, 1640 cm^{-1}. ^{1}H NMR (300 MHz, d_6-DMSO) δ 1.74 (s, 6H, $AdCH_2$), 2.05 (s, 3H, AdCH), 2.16 (s, 6H, $AdCH_2$), 6.91 (d, J = 8.1 Hz, 1H, 5′-ArH), 7.24 (d, J = 8.5 Hz, 1H, 6′-ArH), 7.27 (s, 1H, 2′-ArH), 7.62 (d, J = 8.4 Hz, 1H, 7-NapH), 8.16 (d, J = 8.5 Hz, 2H, 4,8-NapH), 8.37 (d, J = 9.1 Hz, 1H, 3-NapH), 8.68 (s, 1H, 1-NapH), 9.62 ppm (s, 1H, OH). MALDI−FTMS (HRMS) calcd $C_{27}H_{26}ClO_2$ (MH^+) 432.1492, found 432.1502.

Computational Studies. Generation of an RARγ LBD Model for Docking and Simulations. An all-H representation of the RARγ LBD was generated using the XLEAP module of AMBER6[110] and the 9-*cis*-RA (**5**)-bound holo-RARγ LBD crystal structure[65] (PDB entry 3LBD). The initial all-atom model was energy-minimized with a small number of steps (100 steepest descents plus 1900 conjugate-gradient) to remove large initial repulsions in atomic positions as evaluated by the AMBER force-field compared to crystal structure contacts.

Short molecular dynamics (MD) equilibration of the model at constant temperature was performed to provide additional structure relaxation and establish reasonable hydrogen-bonding patterns in the vicinity of the LBP. The model was equilibrated at 300 K with decreasing harmonic constraints over a 20-ps time interval using a 1-femtosecond integration time-step followed by a 70-ps unconstrained equilibration. All bonds involving hydrogens were constrained using SHAKE.[111] The model was then converted to a polar-H representation using AMBER41 for energy-based docking using AUTODOCK 3.0.[112]

Energy-Based Docking. Energy-based docking of flexible AHPN (**1**), 5-Cl-AHPN (**2**), 3-Cl-AHPC (**9**), 3-A-AHPC (**10**), and AHPC (**11**) in the rigid RARγ model was performed using the LGA[113] approach embodied in AUTODOCK 3.0. The LGA docking parameters were: mutation rate, 0.02; crossover rate, 0.80; maximum number of generations, 2.7×10^4; elitism, 1; and local search frequency, 0.06. The lowest energy-binding mode was investigated in short exploratory dynamics employing AMBER6 and an all-atom representation to examine differential ligand effects on RARγ.[114] Charge parametrization for all ligands was derived from restrained electrostatic potential fits derived from DFT computations at ligand optimized geometries.[115]

MD Model Equilibration. MD equilibrations of the all-atom model representations of AHPN (**1**), 5-Cl-AHPN (**2**), 3-A-AHPC (**10**), and AHPC (**11**) docked to the RARγ LBD at constant temperature were performed using a 1-fs integration time-step with constraint of all bonds involving hydrogens employing SHAKE. Coordinates were saved every 0.250 ps for subsequent analysis. The nonbonded pair list was updated every 10 steps. A radial screened dielectric constant (D = r) was employed. Production dynamics was performed for 300 ps to make initial probes of the different potential effects of ligand groups on receptor conformation in the neighborhood of the LBP. To permit a critical comparison of the dynamics of AHPC and 3-A-AHPC in the RARγ LBD with reasonable damping of surface fluctuations, following the identification of low-energy docking modes, the docked lowest-energy conformations of the RARγ LBD−AHPC and 3-A-AHPC complexes were solvated within a large box comprised of 4014 waters and having the initial dimensions of 70 Å × 60 Å × 60 Å. After an initial short 50-ps equilibration at constant volume and a 100-ps equilibration at constant pressure, the system was subjected to 300 ps of production dynamics at 300 K. Periodic boundary conditions were employed with a particle-mesh Ewald summation to provide realistic boundary forces and eliminate the distorting effects of potential truncation.

Density Functional Theory (DFT) Exploration of Inter-ring Torsional Potential Surfaces. AHPN (**1**), 5-Cl-AHPN (**2**), 3-Cl-AHPC (**9**), 3-A-AHPC (**10**), and AHPC (**11**) torsional relaxed potential surfaces were computed using the nonlocal B3LYP DFT functional and a 6-31G** basis set. Optimizations employed Jaguar 4.1 (Schrodinger), default self-consistent field (SCF), and geometric convergence criteria. Unconstrained geometry optimization was performed at each of the parametrically varied torsional angles.

Biology. Reagents. *trans*-RA (**4**) and tryspin-TPCK were purchased from Sigma, and [11,12-$^3H_2$]9-*cis*-retinoic acid (43 Ci/mmol) from Amersham. 4-(5′,6′,7′,8′-Tetrahydro-5′,5′,8′,8′-tetramethyl-2′-anthracenyl)benzoic acid (TTAB, **21**)[71] and the 2-substituted 1,3-dithiolane **22**[70] were synthesized as previously described, as were [5,5′-$^3H_2$]6-[3′-(1-adamantyl)-4′-hydroxyphenyl]-2-naphthalenecarboxylic acid, AHPN (**1**), (*E*)-4-[3′-(1-adamantyl)-4′-hydroxyphenyl]-3-chlorocinnamic acid (3-Cl-AHPC, **9**), and 9-*cis*-RA (**5**).[4,39,40,116,117]

AHPN Analogues. Both agonists and antagonists were dissolved in Me_2SO prior to addition to media. The final concentration of Me_2SO was 0.1% for cancer and leukemia cells. All experiments were conducted in triplicate.

Radioligand Binding and DPSA. DPSA studies using [^{35}S]RARγ and LBD competition radioligand-binding experiments were conducted using bacterially expressed RARs (as GST-fusion proteins) and $(His)_6$−RXRα as described.[70]

GST-Pulldown Assays. Experiments were performed as previously described using GST-p300 1−450 or GST-NCoR 2110−2453 fusion proteins and [^{35}S]methionine-labeled hRARγ LBD prepared by in vitro translation.[70]

Plasmids. Expression vectors for RARγ, RXRα, and the reporter gene $(TREpal)_2$-*tk*-CAT have been described.[118]

Receptor Transcriptional Activation in Cotranfected Cells. CV-1 cells were routinely maintained in DMEM, supplemented with 10% fetal calf serum (FCS), 100 units/mL of penicillin, and 100 μg/mL of streptomycin. For transfection assays, cells were seeded at 1.0×10^5 cells/mL in 24-well plates for 16−24 h before transfection. Cells were then transfected using the calcium chloride precipitation method[119] with either $(TREpal)_2$-*tk*-CAT (200 μg) alone or with the RARγ vector (100 μg) or RXRα vector (20 μg). Cells were cotransfected with β-galactosidase (β-gal) expression vector (pCH 110, Amersham Biosciences) and carrier DNA (pBluescript, Stratagene) to a final concentration of 1000 μg/well. Following transfection for 20 h, the medium was changed to DMEM containing 5% charcoal-stripped FCS, and cells were treated for 24 h with an AHPN analogue or retinoid. Chloramphenicol acetyl transferase (CAT) activity was normalized to β-gal activity to standardize for transfection efficiency.

Cell Lines. Retinoid-resistant MDA-MB-231 and MDA-MB-468 breast cancer and H292 lung cancer and retinoid-sensitive H460 lung and LNCaP prostate cancer cell lines were obtained from the American Type Cell Collection. Retinoid-resistant HR-60R leukemia cells were a gift from Dr. Stephen Collins

(University of Washington, Seattle, WA). Cells were cultured as described below.

Cell Proliferation. MDA-MB-468 cells (1.0×10^5 cells) were seeded in DMEM/F12 medium (Invitrogen Life Technologies) supplemented with 5% fetal bovine serum and 25 μg per mL of gentamicin in Petri dishes or 6-well plates. After 24 h, 3-A-AHPC (**10**) (2.0×10^{-6} M final concentration) and/or 3-Cl-AHPC (**9**) (0.5×10^{-6} M) or vehicle alone were added. Cells were harvested at the times indicated in the figures, and living cell numbers were assessed using a commercial colorimetric assay for the mitochondrial dehydrogenase cleavage of water-soluble 3-(4,5-dimethylthiazol-2-yl)-2,5-diphenyltetrazolium bromide (Sigma-Aldrich) according to the manufacturer's directions. H460 and H292 lung cancer and LNCaP prostate cancer cell lines were grown in RPMI 1640 supplemented with 10% FCS.

Apoptosis. At 24 h after seeding with 1.0×10^5 MDA-MB-468 cells, agonist (0.5×10^{-6} M final concentration) or antagonist (2.0×10^{-6} M) alone or the combination was added, and incubations were continued for 48 or 72 h. Cells were then harvested, and the relative number of apoptotic cells was assessed after fixing and acridine orange staining by counting 200-cell fields for the presence of nuclear fragmentation as previously described.[3]

H460 cells (5×10^5) were treated with 1.0×10^{-6} M 5-Cl-AHPN (**2**) or 3-Cl-AHPC (**9**) alone or combined with $1.0 \times 10^{-}$,[6] $2.5 \times 10^{-}$,[6] or 5.0×10^{-6} M 3-A-AHPC (**10**). After 36 h, cells were trypsinized, then washed with phosphate-buffered saline (PBS, pH 7.4). After fixation with 3.7% paraformaldehyde, cells were washed (PBS) and stained with 4,6-diamidino-2-phenylindole (DAPI, 50 μg/mL) to visualize nuclei by fluorescent microscopy.[38] Cells displaying nuclear morphology characteristic of apoptosis were scored in samples of at least 600 cells. Apoptosis (%) was expressed as the ratio of apoptotic cells to total cells × 100.

Western Blotting. MDA-MB-468 cells (1.0×10^5) were treated for 72 h with a proapoptotic AHPN (0.5×10^{-6} M final concentration) or antagonist **3** (2.0×10^{-6} M) alone or combined. Cells were lysed, and Western blots were performed on the lysates using anti-$p21^{WAF1/CIP1}$ antibody (Transduction Laboratories) and β-actin as the loading control as previously described.[4]

RNA Preparation and Northern Blotting. Total RNA samples were prepared by the guanidine hydrochloride/ultracentrifugation method.[119] Total RNA (30 μg) from cancer cells treated with or without 1.0×10^{-6} M 5-Cl-AHPN (**2**) alone or combined with 1.0×10^{-6} M or 5.0×10^{-6} M 3-A-AHPC (**10**) for 4 h was fractionated on 1% agarose gels. The fractionated RNA was transferred to nylon filters and probed with ^{32}P-labeled TR3 LBD cDNA.[118] Ethidium bromide-stained ribosomal RNA was used as the loading control.

Ligand Binding. Nuclear extracts were prepared from HL-60R cells (1.0×10^5) as we previously described.[4] [5,5′-$^3H_2$]-AHPN[4] (10×10^{-9} M, 150 000 dpm) was added to the nuclear extracts in the presence and absence of 20×10^{-6} M nonlabeled AHPN (**1**) or 3-A-AHPC (**10**) or vehicle alone. After a 90-min incubation at 22 °C, free ligand was separated from bound ligand on a 0.5-cm × 4.0-cm column of fine-mesh G25 Sephadex (Pharmacia) by elution with binding buffer.[4] The bound fraction was counted as we described.[4]

Acknowledgment. These studies were supported by NCI grant P01 CA51993 (M.I.D., M.L., J.A.F., and X.Z.), California Breast Cancer Research Program grant 8WB-017 (M.I.D., D.H.L., X.Z.), and California Tobacco-Related Diseases Research Program grants 6RT-0212A (M.I.D.) and 11RT-0081 (X.Z., M.I.D.). N.B.-S. was supported by a postdoctoral fellowship from the California Breast Cancer Research Program. D.L.H. acknowledges the NSF supercomputer grant award MCB030032 at the Pittsburgh Computer Center. Special thanks go to Cynthia Cook and Helen Hansen for their help with preparing this manuscript.

Appendix

Acromyns and/or code numbers for 6-[3′-(1-adamantyl)-4′-hydroxyphenyl)]-2-naphthalenecarboxylic acid, its analogues, and retinoids are listed in the legend for Figure 1. Other abbreviations are 1-Ad, 1-adamantyl; 3-A, 3-(3′-acetamidopropyloxy); Bcl-2, diffuse B-cell lymphoma cytoprotective protein; CAT, chloramphenicol acetyl transferase; CPK, Corey−Pauling−Kortum; CV-1, African green monkey kidney cell line; DAPI, 4,6-diamidino-2-phenylindole; DPSA, differential protease sensitivity assay; DTF, density functional theory; FCS, fetal calf serum; GST, glutathione *S*-transferase; LBD, ligand-binding domain; LGA, Larmarkian Genetic Algorithm; LBP, ligand-binding pocket; NCoR, nuclear receptor corepressor protein; $p21^{WAF/CIP1}$, 21-kDa wild-type p53-activated fragment 1 or cyclin-dependent kinase-2-interacting protein; p300, an acetyl transferase and transcriptional coactivator of nuclear receptors; PBS, phosphate-buffered saline, pH 7.4; RA, retinoic acid; RAR, retinoic acid receptor; RXR, retinoid X receptor; TPCK-trypsin, bovine pancreas trypsin treated with *N*-(*p*-tosyl)-L-phenylanlanine chloromethyl ketone; TREpal, palindromic RAR- and RXR-responsive element; *tk*, thymidine kinase promoter; TTN, 5,6,7,8-tetrahydro-5,5,8,8-tetramethyl-2-naphthalene.

Supporting Information Available: Elemental analyses for compounds **45** and **46**. This material is available free of charge via the Internet at http://pubs.acs.org.

References

(1) Bernard, B. A.; Bernardon, J. M.; Delescluse, C.; Martin, B.; Lenoir, M. C.; Maignan, J.; Charpentier, B.; Pilgrim, W. R.; Reichert, U.; Shroot, B. Identification of synthetic retinoids with selectivity for human nuclear retinoic acid receptor gamma. *Biochem. Biophys. Res. Commun.* **1992**, *186*, 977−983.

(2) Shao, Z.-M.; Dawson, M. I.; Li, X. S.; Rishi, A. K.; Sheikh, M. S.; Han, Q. X.; Ordonez, J. V.; Shroot, B.; Fontana, J. A. p53 independent G_0/G_1 arrest and apoptosis induced by a novel retinoid in human breast cancer cells. *Oncogene* **1995**, *11*, 493−504.

(3) Li, X.-S.; Rishi, A. K.; Shao, Z. M.; Dawson, M. I.; Jong, L.; Shroot, B.; Reichert, U.; Ordonez, J.; Fontana, J. A. Posttranscriptional regulation of $p21^{WAF1/CIP1}$ expression in human breast carcinoma cells. *Cancer Res.* **1996**, *56*, 5055−5062.

(4) Fontana, J. A.; Dawson, M. I.; Leid, M.; Rishi, A. K.; Zhang, Y.; Hsu, C.-A.; Lu, J. S.; Peterson, V. J.; Jong, L.; Hobbs, P.; Chao, W.-R.; Shroot, B.; Reichert, U. Identification of a unique binding protein specific for a novel retinoid inducing cellular apoptosis. *Int. J. Cancer* **2000**, *86*, 474−479.

(5) Dawson, M. I.; Hobbs, P. D.; Peterson, V. J.; Leid, M.; Lange, C. W.; Feng, K. C.; Chen, G.; Gu, J.; Li, H.; Kolluri, S. K.; Zhang, X.; Zhang, Y.; Fontana, J. A. Apoptosis induction in cancer cells by a novel analogue of 6-[3-(1-adamantyl)-4-hydroxyphenyl]-2-naphthalenecarboxylic acid lacking retinoid receptor transcriptional activation activity. *Cancer Res.* **2001**, *61*, 4723−4730.

(6) Mangelsdorf, D. J.; Umesono, K.; Evans, R. M. The retinoid receptors. In *The Retinoids: Biology, Chemistry, and Medicine*; Sporn, M. B., Roberts, A. B., Goodman, D. S., Eds.; Raven Press: New York, 1994; pp 319−349.

(7) Dawson, M. I.; Chao, W. R.; Pine, P.; Jong, L.; Hobbs, P. D.; Rudd, C. K.; Quick, T. C.; Niles, R. M.; Zhang, X.-K.; Lombardo, A.; Ely, K. R.; Shroot, B.; Fontana, J. A. Correlation of retinoid binding affinity to RARα with retinoid inhibition of growth of estrogen receptor-positive MCF-7 mammary carcinoma cells. *Cancer Res.* **1995**, *55*, 4446−4451.

(8) Fitzgerald, P.; Teng, M.; Chandraratna, R. A. S.; Heyman, R. A.; Allegretto, E. A. Retinoic acid receptor α expression correlates with retinoid-induced growth inhibition of human breast cancer cells regardless of estrogen receptor status. *Cancer Res.* **1997**, *57*, 2642−2650.

(9) Chao, W. R.; Hobbs, P. D.; Jong, L.; Zhang, X.-K.; Zheng, Y.; Wu, Q.; Shroot, B.; Dawson, M. I. Effects of receptor class- and subtype-selective retinoids and an apoptosis-inducing retinoid on the adherent growth of the NIH:OVCAR-3 ovarian cancer cell line in culture. *Cancer Lett.* **1997**, *115*, 1−7.

(10) Li, H.; Kolluri, S. K.; Gu, J.; Dawson, M. I.; Cao, X.; Hobbs, P. D.; Lin, B.; Chen, G.; Lu, J.; Lin, F.; Xie, Z.; Fontana, J. A.; Reed, J. C.; Zhang, X. Cytochrome *c* release and apoptosis induced by mitochondrial targeting of nuclear orphan receptor TR3. *Science* **2000**, *289*, 1159−1164.
(11) Milbrandt, J. Nerve growth factor induces a gene homologous to the glucocorticoid receptor gene. *Neuron* **1988**, *1*, 183−188.
(12) Chang, C.; Kokontis, J. Identification of a new member of the steroid receptor super-family by cloning and sequence analysis. *Biochem. Biophys. Res. Commun.* **1988**, *155*, 971−977.
(13) Hazel, T. G.; Nathans, D.; Lau, L. F. A gene inducible by serum growth factors encodes a member of the steroid and thyroid hormone receptor superfamily. *Proc. Natl. Acad. Sci. U.S.A.* **1988**, *85*, 8444−8448.
(14) Leid, M.; Kastner, P.; Lyons, R.; Nakshatri, H.; Saunders: M.; Zacharewski, T.; Chen, J.-Y.; Staub, A.; Garnier, J.-M.; Mader, S.; Chambon, P. Purification, cloning, and RXR identity of the HeLa cell factor with which RAR or TR heterodimerizes to bind target sequences efficiently. *Cell* **1992**, *68*, 377−395.
(15) Green, D. R.; Reed, J. C. Mitochondria and apoptosis. *Science* **1998**, *281*, 1309−1312.
(16) Lin, B.; Kolluri, S. K.; Lin, F.; Liu, W.; Han, Y. H.; Cao, X.; Dawson, M. I.; Reed, J. C.; Zhang, X.-K. Conversion of Bcl-2 from protector to killer by interaction with nuclear orphan receptor Nur77/TR3. *Cell* **2004**, *116*, 527−540.
(17) Armstrong, R. B.; Ashenfelter, K. O.; Eckhoff, C.; Levin, A. A.; Shapiro, S. S. General and reproductive toxicology of retinoids. In *The Retinoids: Biology, Chemistry, and Medicine*; Sporn, M. B., Roberts, A. B., Goodman, D. S., Eds.; Raven Press: New York, 1994; pp 545−572.
(18) Graf, N.; Riesinger, P.; Reinhard, H. Retinoids in the treatment of acute promyelocytic leukemia. Review of the literature. *Klin. Padiatr.* **1995**, *207*, 43−47.
(19) Selleri, C.; Pane, F.; Notaro, R.; Catalano, L.; Santoro, L. E.; Luciano, L.; Frigeri, F.; Salvatore, F.; Rotoli, B. All-*trans*-retinoic acid (ATRA) responsive skin relapses of acute promyelocytic leukaemia followed by ATRA-induced *pseudotumour cerebri*. *Br. J. Haematol.* **1996**, *92*, 937−940.
(20) De Botton, S.; Dombret, H.; Sanz, M.; Miguel, J. S.; Caillot, D.; Zittoun, R.; Gardembas, M.; Stamatoulas, A.; Conde, E.; Guerci, A.; Gardin, C.; Geiser, K.; Makhoul, D. C.; Reman, O.; de la Serna, J.; Lefrere, F.; Chomienne, C.; Chastang, C.; Degos, L.; Fenaux, P. Incidence, clinical features, and outcome of all *trans*-retinoic acid syndrome in 413 cases of newly diagnosed acute promyelocytic leukemia. The European APL Group. *Blood* **1998**, *92*, 2712−2718.
(21) Levi, I.; Raanani, P.; Shalmon, B.; Schiby-Brilliant, R.; Ben-Bassat, I. Acute neutrophilic dermatosis induced by all-*trans*-retinoic acid treatment for acute promyelocytic leukemia. *Leuk. Lymphoma* **1999**, *34*, 401−404.
(22) Wu, W.; Sun, G.; Zhou, R.; Li, X.; Shen, Z.; Wang, Z. The relationship between the levels of granulocyte colony-stimulating factor and leukocytosis induced by all-trans retinoic acid in acute promyelocytic leukemia. *Chin. Med. J. (Engl.)* **1999**, *112*, 1085−1087.
(23) Tommasino, C.; De Felice, L.; Colombo, S.; Salaris, D.; Capocasa, T.; Giudici, D. Retinoic acid syndrome. Severe respiratory insufficiency treated with CPAP. *Minerva Anestesiol.* **2000**, *66*, 555−559.
(24) Duvic, M.; Hymes, K.; Heald, P.; Breneman, D.; Martin, A. G.; Myskowski, P.; Crowley, C.; Yocum, R. C. Bexarotene is effective and safe for treatment of refractory advanced-stage cutaneous T-cell lymphoma: Multinational phase II−III trial results. *J. Clin. Oncol.* **2001**, *19*, 2456−2471.
(25) Martín del Pozo, M.; Cisneros de la Fuente, E.; Solano, F.; Martín, M. L.; de la Serna, J. The retinoic acid syndrome, a complication of acute promyelocytic leukemia therapy. *An. Med. Intern.* **2001**, *18*, 195−200.
(26) Goncalves, A.; Camerlo, J.; Bun, H.; Gravis, G.; Genre, D.; Bertucci, F.; Resbeut, M.; Pech-Gourg, F.; Durand, A.; Maraninchi, D.; Viens, P. Phase II study of a combination of cisplatin, all-*trans*-retinoic acid and interferon-α in squamous cell carcinoma: Clinical results and pharmacokinetics. *Anticancer Res.* **2001**, *21*, 1431−1437.
(27) Khuri, F. R.; Rigas, J. R.; Figlin, R. A.; Gralla, R. J.; Shin, D. M.; Munden, R.; Fox, N.; Huyghe, M. R.; Kean, Y.; Reich, S. D.; Hong, W.-K. Multi-institutional Phase I/II trial of oral bexarotene in combination with cisplatin and vinorelbine in previously untreated patients with advanced nonsmall-cell lung cancer. *J. Clin. Oncol.* **2001**, *19*, 2626−2637.
(28) Park, C. J.; Bae, Y. D.; Choi, J. Y.; Heo, P. S.; Lee, K. S.; Park, Y. S.; Lee, J. A. Sweet's syndrome during the treatment of acute promyelocytic leukemia with all-trans retinoic acid. *Korean J. Intern. Med.* **2001**, *16*, 218−221.
(29) Shin, D. M.; Glisson, B. S.; Khuri, F. R.; Clifford, J. L.; Clayman, G.; Benner, S. E.; Forastiere, A. A.; Ginsberg, L.; Liu, D.; Lee, J. J.; Myers, J.; Goepfert, H.; Lotan, R.; Hong, W. K.; Lippman, S. M. Phase II and biologic study of interferon α, retinoic acid, and cisplatin in advanced squamous skin cancer. *J. Clin. Oncol.* **2002**, *20*, 364−370.
(30) Standeven, A. M.; Teng, M.; Chandraratna, R. A. S. Lack of involvement of retinoic acid receptor α in retinoid-induced skin irritation in hairless mice. *Toxicol. Lett.* **1997**, *92*, 231−240.
(31) Iulianella, A.; Lohnes, D. Contribution of retinoic acid receptor γ to retinoid-induced craniofacial and axial defects. *Dev. Dyn.* **1997**, *209*, 92−104.
(32) Look, J.; Landwehr, J.; Bauer, F.; Hoffmann, A. S.; Bluethmann, H.; LeMotte, P. Marked resistance of RARγ-deficient mice to the toxic effects of retinoic acid. *Am. J. Physiol.* **1995**, *269*, E91-E98.
(33) Reczek, P. R.; Ostrowski, J.; Yu, K. L.; Chen, S.; Hammer, L.; Roalsvig, T.; Starrett, J. E., Jr.; Driscoll, J. P.; Whiting, G.; Spinazze, P. G. Role of retinoic acid receptor γ in the Rhino mouse and rabbit irritation models of retinoid activity. *Skin Pharmacol.* **1995**, *8*, 292−299.
(34) Sheikh, M. S.; Shao, Z.-M.; Li, X.-S.; Dawson, M. I.; Jetten, A. M.; Wu, S.; Conley, B. A.; Garcia, M.; Rochefort, H.; Fontana, J. A. Retinoid-resistant estrogen receptor-negative human breast carcinoma cells transfected with retinoic acid receptor-α acquire sensitivity to growth inhibition by retinoids. *J. Biol. Chem.* **1994**, *269*, 21440−21447.
(35) Swisshelm, K.; Ryan, K.; Lee, X.; Tsou, H. C.; Peacocke, M.; Sager, R. Down-regulation of retinoic acid receptor β in mammary carcinoma cell lines and its up-regulation in senescing normal mammary epithelial cells. *Cell Growth Differ.* **1994**, *5*, 133−141.
(36) Li, X.-S.; Shao, Z.-M.; Sheikh, M. S.; Eiseman, J. L.; Sentz, D.; Jetten, A. M.; Chen, J.-C.; Dawson, M. I.; Aisner, S.; Rishi, A. K.; Fontana, J. A. Retinoic acid nuclear receptor β (RARβ) inhibits breast carcinoma anchorage independent growth. *J. Cell. Physiol.* **1995**, *165*, 449−458.
(37) Lotan, R.; Xu, X. C.; Lippman, S. M.; Ro, J. Y.; Lee, J. S.; Lee, J. J.; Hong, W.-K. Suppression of retinoic acid receptor-β in premalignant oral lesions and its up-regulation by isotretinoin. *New Engl. J. Med.* **1995**, *332*, 1405−1410.
(38) Liu, Y.; Lee, M.-O.; Wang, H.-G.; Li, Y.; Hashimoto, Y.; Klaus, M.; Reed, J. C.; Zhang, X. RARβ mediates the growth-inhibitory effect of retinoic acid by promoting apoptosis in human breast cancer cells. *Mol. Cell. Biol.* **1996**, *16*, 1138−1149.
(39) Zhang, Y.; Dawson, M. I.; Mohammad, R.; Rishi, A. K.; Farhana, L.; Feng, K. C.; Leid, M.; Peterson, V.; Zhang, X.-K.; Edelstein, M.; Eilander, D.; Biggar, S.; Wall, N.; Reichert, U.; Fontana, J. A. Induction of apoptosis of human B-CLL and ALL cells by a novel retinoid and its nonretinoidal analogue. *Blood* **2002**, *100*, 2917−2925.
(40) Zhang, Y.; Dawson, M. I.; Ning, Y.; Polin, L.; Parchment, R. E.; Corbett, T.; Mohamed, A. N.; Feng, K. C.; Farhana, L.; Rishi, A. K.; Hogge, D.; Leid, M.; Peterson, V. J.; Zhang, X.-K.; Mohammad, R.; Lu, J. S.; Willman, C.; VanBuren, E.; Biggar, S.; Edelstein, M.; Eilender, D.; Fontana, J. A. Induction of apoptosis in retinoid-refractory acute myelogenous leukemia by a novel AHPN analogue. *Blood* **2003**, *102*, 3743−3752.
(41) Schiff, L. J.; Okamura, W. H.; Dawson, M. I.; Hobbs, P. D. Structure-biological activity relationships of new synthetic retinoids on epithelial differentiation of cultured hamster trachea. In *Chemistry and Biology of Synthetic Retinoids*; Dawson, M. I., Okamura, W. H., Eds.; CRC Press: Boca Rotan, 1990; pp 302−363.
(42) Dawson, M. I.; Chan, R. L.-S.; Derdzinski, K.; Hobbs, P. D.; Chao, W.-R.; Schiff, L. J. Synthesis and pharmacological activity of 6-[(*E*)-2-(2,6,6-trimethyl-1-cyclohexen-1-yl)ethen-1-yl]- and 6-(1,2,3,4-tetrahydro-1,1,4,4-tetramethyl-6-naphthyl)-2-naphthalenecarboxylic acids. *J. Med. Chem.* **1983**, *26*, 1653−1656.
(43) Schiff, L. J.; Moore, S. J.; Dawson, M. I.; Hobbs, P. D.; Chan, R. L.-S.; Derdzinski, K. Biological activity of aromatic retinoid acid analogues in hamster tracheal organ culture. In *In Vitro Models of Respiratory Epithelium*; Schiff, L. J., Ed.; CRC Press: Boca Raton, FL, 1986; pp 51−83.
(44) Cincinelli, R.; Dallavalle, S.; Merlini, L.; Penco, S.; Pisano, C.; Carminati, P.; Giannini, G.; Vesci, L.; Gaetano, C.; Illy, B.; Zuco, V.; Supino, R.; Zunino, F. A novel atypical retinoid endowed with proapoptotic and antitumor activity. *J. Med. Chem.* **2003**, *46*, 909−912.
(45) Dawson, M. I.; Chao, W.-R.; Hobbs, P. D.; Delair, T. The inihibitory effects of retinoids on the induction of ornithine decarboxylase and the promotion of tumors in mouse epidermis. In *Chemistry and Biology of Synthetic Retinoids*; Dawson, M. I., Okamura, W. H., Eds.; CRC Press: Boca Rotan, 1990; pp 385−466.
(46) Dawson, M. I.; Park, J.-H.; Chen, G.; Chao, W.; Dousman, L.; Waleh, N.; Hobbs, P. D.; Jong, L.; Toll, L.; Zhang, X.; Gu, J.; Agadir, A.; Merchant, J. L.; Bai, L.; Verma, A. K.; Thacher, S. M.; Chandraratna, R. A. S.; Shroot, B.; Hill, D. L. Retinoic acid

(RA) receptor transcriptional activation correlates with inhibition of 12-*O*-tetradecanoylphorbol-13-acetate-induced ornithine decarboxylase (ODC) activity by retinoids: A potential role for *trans*-RA-induced ZBP-89 in ODC inhibition. *Int. J. Cancer* **2001**, *91*, 8−21.

(47) Dawson, M. I.; Hobbs, P. D.; Stein, R. B.; Berger, T. S.; Heyman, R. A. Interaction of retinoids with retinoic nuclear receptor isoforms. In *Retinoids: New Trends in Research and Clinical Applications*; Livrea, M. A., Packer, L., Eds.; Marcel Dekker: New York, 1992; pp 205−221.

(48) Lehmann, J. M.; Dawson, M. I.; Hobbs, P. D.; Husmann, M.; Pfahl, M. Identification of retinoids with nuclear receptor subtype-selective activities. *Cancer Res.* **1991**, *51*, 4804−4809.

(49) Dawson, M. I.; Zhang, X.; Hobbs, P. D.; Jong, L. Synthetic retinoids and their usefulness in biology and medicine. In *Vitamin A and Retinoids: An Update of Biological Aspects and Clinical Applications*; Livrea, M. A., Ed.; Birkhäuser Verlag: Basel, Switzerland, 2000; pp 161−196.

(50) Lehmann, J. M.; Jong, L.; Fanjul, A.; Cameron, J. F.; Liu, X. P.; Haefner, P.; Dawson, M. I.; Pfahl, M. A novel class of retinoids, selective for retinoid X receptor response pathways. *Science* **1992**, *258*, 1944−1946.

(51) Dawson, M. I.; Jong, L.; Hobbs, P. D.; Cameron, J. F.; Chao, W.-R.; Pfahl, M.; Lee, M.-O.; Shroot, B. Conformational effects on retinoid receptor selectivity. 2. Effects of retinoid bridging group on retinoid X receptor activity and selectivity. *J. Med. Chem.* **1995**, *38*, 3368−3383.

(52) Dawson, M. I.; Cameron, J. F.; Hobbs, P. D.; Jong, L.; Pfahl, M.; Zhang, X.; Lehmann, J. M. (SRI International and The Burnham Institute, formerly La Jolla Cancer Research Foundation). Bridged bicyclic aromatic compounds and their use in modulating gene expression of retinoid receptors. U.S. Patent 5,837,725, 1998.

(53) Dawson, M. I.; Hobbs, P. D.; Jong, L.; Xiao, D.; Chao, W.-R.; Pan, C.; Zhang, X.-K. sp2-bridged diaryl retinoids: Effects of bridge-region substitution on retinoid X receptor (RXR) selectivity. *Bioorg. Med. Chem. Lett.* **2000**, *10*, 1307−1310.

(54) Dawson, M. I.; Zhang, X.-K. Discovery and design of retinoic acid receptor and retinoid X receptor class- and subtype-selective synthetic analogues of all-*trans*-retinoic acid and 9-*cis*-retinoic acid. *Curr. Med. Chem.* **2002**, *9*, 623−637.

(55) Boehm, M. F.; Zhang, L.; Zhi, L.; McClurg, M. R.; Berger, E.; Wagoner, M.; Mais, D. E.; Suto, C. M.; Davies, J. A.; Heyman, R. A.; Nadzan, A. M. Design and synthesis of potent retinoid X receptor selective ligands that induce apoptosis in leukemia cells. *J. Med. Chem.* **1995**, *38*, 3146−3155.

(56) Beard, R. L.; Colon, D. F.; Song, T. K.; Davies, P. J.; Kochhar, D. M.; Chandraratna, R. A. S. Synthesis and structure−activity relationships of retinoid X receptor selective diaryl sulfide analogues of retinoic acid. *J. Med. Chem.* **1996**, *39*, 3556−3563.

(57) Dawson, M. I.; Chao, W. R.; Hobbs, P. D.; Zhang, X.-K. Effects of *trans*-retinoic acid, 9-*cis*-retinoic acid, 1α,25-(dihydroxy)-vitamin D_3 and a novel apoptosis-inducing retinoid on breast cancer and endothelial cell growth. *Cancer Lett.* **1998**, *133*, 1−8.

(58) Robertson, K. A.; Emami, B.; Collins, S. J. Retinoic acid-resistant HL-60R cells harbor a point mutation in the retinoic acid receptor ligand-binding domain that confers dominant negative activity. *Blood* **1992**, *80*, 1885−1889.

(59) Ota, E.; Shimozawa, J. T. Substitution reactions of phenanthrols. XII. Conversion of phenanthrols to the corresponding chloro- and bromophenanthrenes and their dipole moment measurements. *Nippon Kagaku Kaishi* **1987**, *4*, 757−761.

(60) Dawson, M. I.; Cavasotto, C. N.; Hobbs, P. D.; Jong, L.; Feng, K.-C.; Lui, H.; Abagyan, R.; Zhang, X. Synthesis and biological activity of an RXR antagonist. Presented at the 93rd Annual AACR National Meeting, San Francisco, CA, 2002.

(61) Brzozowski, A. M.; Pike, A. C.; Dauter, Z.; Hubbard, R. E.; Bonn, T.; Engstrom, O.; Ohman, L.; Greene, G. L.; Gustafsson, J.-A.; Carlquist, M. Molecular basis of agonism and antagonism in the oestrogen receptor. *Nature* **1997**, *389*, 753−758.

(62) Pike, A. C.; Brzozowski, A. M.; Hubbard, R. E.; Bonn, T.; Thorsell, A. G.; Engstrom, O.; Ljunggren, J.; Gustafsson, J. A.; Carlquist, M. Structure of the ligand-binding domain of oestrogen receptor β in the presence of a partial agonist and a full antagonist. *EMBO J.* **1999**, *18*, 4608−4618.

(63) Delabre, K.; Guiochon-Mantel, A.; Milgrom, E. In vivo evidence against the existence of antiprogestins disrupting receptor binding to DNA. *Proc. Natl. Acad. Sci. U.S.A.* **1993**, *90*, 4421−4425.

(64) Brand, C.; Ségard, P.; Plouvier, P.; Formstecher, P.; Danzé, P. M.; Lefebvre, P. Selective alteration of gene expression in response to natural and synthetic retinoids. *BMC Pharmacol.* **2002**, *2*, 13.

(65) Klaholz, B. P.; Renaud, J. P.; Mitschler, A.; Zusi, C.; Chambon, P.; Gronemeyer, H.; Moras, D. Conformational adaptation of agonists to the human nuclear receptor RARγ. *Nat. Struct. Biol.* **1998**, *5*, 199−202.

(66) Apfel, C.; Bauer, F.; Crettaz, M.; Forni, L.; Kamber, M.; Kaufmann, F.; LeMotte, P.; Pirson, W.; Klaus, M. A retinoic acid receptor α antagonist selectively counteracts retinoic acid effects. *Proc. Natl. Acad. Sci. U.S.A.* **1992**, *89*, 7129−7133.

(67) Lala, D. S.; Mukherjee, R.; Schulman, I. G.; Koch, S. S.; Dardashti, L. J.; Nadzan, A. M.; Croston, G. E.; Evans, R. M.; Heyman, R. A. Activation of specific RXR heterodimers by an antagonist of RXR homodimers. *Nature* **1996**, *383*, 450−453.

(68) Arulmozhiraja, S.; Selvin, P. C.; Fujii, T. Structures, potential energy curves, and torsional barrier heights for selected polychlorinated biphenyls: A density functional theory study. *J. Phys. Chem. A* **2002**, *106*, 1765−1769.

(69) Arulmozhiraja, S.; Fujii, T. Torsional barrier, ionization potential, and electron affinity of biphenyl−A theoretical study. *J. Chem. Phys.* **2001**, *115*, 10589−10594.

(70) Peterson, V. J.; Barofsky, E.; Deinzer, M. L.; Dawson, M. I.; Feng, K. C.; Zhang, X.-K.; Madduru, M. R.; Leid, M. Mass-spectrometric analysis of agonist-induced retinoic acid receptor γ conformational change. *Biochem. J.* **2002**, *362*, 173−181.

(71) Dawson, M. I.; Hobbs, P. D.; Derdzinski, K. A.; Chao, W.-R.; Frenking, G.; Loew, G. H.; Jetten, A. M.; Napoli, J. L.; Williams, J. B.; Sani, B. P.; Wille, J. J., Jr.; Schiff, L. J. Effect of structural modifications in the C7−C11 region of the retinoid skeleton on biological activity in a series of aromatic retinoids. *J. Med. Chem.* **1989**, *32*, 1504−1517.

(72) Nielsen, L. L.; Dell, J.; Maxwell, E.; Armstrong, L.; Maneval, D.; Catino, J. J. Efficacy of p53 adenovirus-mediated gene therapy against human breast cancer xenografts. *Cancer Gene Ther.* **1997**, *4*, 129−138.

(73) Sheikh, M. S.; Li, X.-S.; Chen, J. C.; Shao, Z. M.; Ordonez, J. V.; Fontana, J. A. Mechanisms of regulation of WAF1/Cip1 gene expression in human breast carcinoma: Role of p53-dependent and independent signal transduction pathways. *Oncogene* **1994**, *9*, 3407−3415.

(74) Xinarianos, G.; Liloglou, T.; Prime, W.; Sourvinos, G.; Karachristos, A.; Gosney, J. R.; Spandidos, D. A.; Field, J. K. p53 status correlates with the differential expression of the DNA mismatch repair protein MSH2 in nonsmall cell lung carcinoma. *Int. J. Cancer* **2002**, *101*, 248−252.

(75) Campling, B. G.; el-Deiry, W. S. Clinical implications of p53 mutations in lung cancer. *Methods Mol. Med.* **2003**, *75*, 53−77.

(76) Zhang, Y.; Huang, Y.; Rishi, A. K.; Sheikh, M. S.; Shroot, B.; Reichert, U.; Dawson, M. I.; Poirer, G.; Fontana, J. A. Activation of the p38 and JNK/SAPK mitogen-activated protein kinase pathways during apoptosis is mediated by a novel retinoid. *Exp. Cell Res.* **1999**, *247*, 233−240.

(77) Li, Y.; Lin, B.; Agadir, A.; Liu, R.; Dawson, M. I.; Reed, J. C.; Fontana, J. A.; Bost, F.; Hobbs, P. D.; Zheng, Y.; Chen, G.-Q.; Shroot, B.; Mercola, D.; Zhang, X.-K. Molecular determinants of AHPN (CD437)-induced growth arrest and apoptosis in human lung cancer cell lines. *Mol. Cell. Biol.* **1998**, *18*, 4719−4731.

(78) White, E. Life, death, and the pursuit of apoptosis. *Genes Dev.* **1996**, *10*, 1−15.

(79) Green, D.; Kroemer, G. The central executioners of apoptosis: Caspases or mitochondria? *Trends Cell. Biol.* **1998**, *8*, 267−271.

(80) Hsu, C. K. A.; Rishi, A. K.; Li, X.-S.; Dawson, M. I.; Reichert, U.; Shroot, B.; Fontana, J. A. Bcl-X_L expression and its down-regulation by a novel retinoid in breast carcinoma cells. *Exp. Cell Res.* **1997**, *232*, 17−24.

(81) Fanjul, A. N.; Piedrafita, F. J.; Al-Shamma, H.; Pfahl, M. Apoptosis induction and potent antiestrogen receptor-negative breast cancer activity *in vivo* by a retinoid antagonist. *Cancer Res.* **1998**, *58*, 4607−4610.

(82) Rishi, A. K.; Sun, R. J.; Gao, Y.; Hsu, C. K.; Gerald, T. M.; Saeed Sheikh, M.; Dawson, M. I.; Reichert, U.; Shroot, B.; Fornace, A. J., Jr.; Brewer, G.; Fontana, J. A. Posttranscriptional regulation of the DNA damage-inducible gadd45 gene in human breast carcinoma cells exposed to a novel retinoid CD437. *Nucleic Acids Res.* **1999**, *27*, 3111−3119.

(83) Lu, X. P.; Fanjul, A.; Picard, N.; Pfahl, M.; Rungta, D.; Nared-Hood, K.; Carter, B.; Piedrafita, J.; Tang, S.; Fabbrizio, E. Novel retinoid-related molecules as apoptosis inducers and effective inhibitors of human lung cancer cells in vivo. *Nat. Med.* **1997**, *3*, 686−690.

(84) Sun, S.-Y.; Yue, P.; Shroot, B.; Hong, W. K.; Lotan, R. Implication of c-Myc in apoptosis induced by the retinoid CD437 in human lung carcinoma cells. *Oncogene* **1999**, *18*, 3894−3901.

(85) Sun, S.-Y.; Yue, P.; Wu, G. S.; El-Deiry, W. S.; Shroot, B.; Hong, W. K.; Lotan, R. Implication of p53 in growth arrest and apoptosis induced by the synthetic retinoid CD437 in human lung cancer cells. *Cancer Res.* **1999**, *59*, 2829−2833.

(86) Sun, S.-Y.; Yue, P.; Chen, X.; Hong, W. K.; Lotan, R. The synthetic retinoid CD437 selectively induces apoptosis in human lung cancer cells while sparing normal human lung epithelial cells. *Cancer Res.* **2002**, *62*, 2430−2436.

(87) Hsu, C. A.; Rishi, A. K.; Li, X.-S.; Gerald, T. M.; Dawson, M. I.; Schiffer, C.; Reichert, U.; Shroot, B.; Poirer, G. C.; Fontana, J. A. Retinoid induced apoptosis in leukemia cells through a retinoic acid nuclear receptor-independent pathway. *Blood* **1997**, *89*, 4470−4479.
(88) Giannì, M.; de Thé, H. In acute promyelocytic leukemia NB4 cells, the synthetic retinoid CD437 induces contemporaneously apoptosis, a caspase-3-mediated degradation of PML/RARα protein and the PML retargeting on PML-nuclear bodies. *Leukemia* **1999**, *13*, 739−749.
(89) Mologni, L.; Ponzanelli, I.; Bresciani, F.; Sardiello, G.; Bergamaschi, D.; Gianni, M.; Reichert, U.; Rambaldi, A.; Terao, M.; Garattini, E. The novel synthetic retinoid 6-[3-adamantyl-4-hydroxyphenyl]-2-naphthalenecarboxylic acid (CD437) causes apoptosis in acute promyelocytic leukemia cells through rapid activation of caspases. *Blood* **1999**, *93*, 1045−1061.
(90) Oridate, N.; Higuchi, M.; Suzuki, S.; Shroot, B.; Hong, W.-K.; Lotan, R. Rapid induction of apoptosis in human C33A cervical carcinoma cells by the synthetic retinoid 6-[3-(1-adamantyl)-hydroxyphenyl]-2-naphthalenecarboxylic acid (CD437). *Int. J. Cancer* **1997**, *70*, 484−487.
(91) Wan, X.; Duncan, M. D.; Nass, P.; Harmon, J. W. Synthetic retinoid CD437 induces apoptosis of esophageal squamous HET-1A cells through the caspase-3-dependent pathway. *Anticancer Res.* **2001**, *21*, 2657−2663.
(92) Adachi, H.; Adams, A.; Hughes, F. M.; Zhang, J.; Cidlowski, J. A.; Jetten, A. M. Induction of apoptosis by the novel retinoid AHPN in human T-cell lymphoma cells involves caspase-dependent and independent pathways. *Cell Death Differ.* **1998**, *5*, 973−983.
(93) Schadendorf, D.; Worm, M.; Jurgovsky, K.; Dippel, E.; Reichert, U.; Czarnetzki, B. M. Effects of various synthetic retinoids on proliferation and immunophenotype of human melanoma cells in vitro. *Recent Results Cancer Res.* **1995**, *139*, 183−193.
(94) Schadendorf, D.; Kern, M. A.; Artuc, M.; Pahl, H. L.; Rosenbach, T.; Fichtner, I.; Nurnberg, W.; Stuting, S.; von Stebut, E.; Worm, M.; Makki, A.; Jurgovsky, K.; Kolde, G.; Henz, B. M. Treatment of melanoma cells with the synthetic retinoid CD437 induces apoptosis via activation of AP-1 *in vitro*, and causes growth inhibition in xenografts in vivo. *J. Cell Biol.* **1996**, *135*, 1889−1898.
(95) Meister, B.; Fink, F. M.; Hittmair, A.; Marth, C.; Widschwendter, M. Antiproliferative activity and apoptosis induced by retinoic acid receptor-γ selectively binding retinoids in neuroblastoma. *Anticancer Res.* **1998**, *18*, 1777−1786.
(96) Langdon, S. P.; Rabiasz, G. J.; Ritchie, A. A.; Reichert, U.; Buchan, P.; Miller, W. R.; Smyth, J. F. Growth-inhibitory effects of the synthetic retinoid CD437 against ovarian carcinoma models in vitro and in vivo. *Cancer Chemother. Pharmacol.* **1998**, *42*, 429−432.
(97) Holmes, W. F.; Soprano, D. R.; Soprano, K. J. Comparison of the mechanism of induction of apoptosis in ovarian carcinoma cells by the conformationally restricted synthetic retinoids CD437 and 4-HPR. *J. Cell Biochem.* **2003**, *89*, 262−278.
(98) Holmes, W. F.; Soprano, D. R.; Soprano, K. J. Elucidation of molecular events mediating induction of apoptosis by synthetic retinoids using a CD437-resistant ovarian carcinoma cell line. *J. Biol. Chem.* **2002**, *277*, 45408−45419.
(99) Hsu, J. Y.; Pfahl, M. ET-1 expression and growth inhibition of prostate cancer cells: A retinoid target with novel specificity. *Cancer Res.* **1998**, *58*, 4817−4822.
(100) Liang, J. Y.; Fontana, J. A.; Rao, J. N.; Ordonez, J. V.; Dawson, M. I.; Shroot, B.; Wilber, J. F.; Feng, P. Synthetic retinoid CD437 induces S-phase arrest and apoptosis in human prostate cancer cells LNCaP and PC-3. *Prostate* **1999**, *38*, 228−236.
(101) Lu, X. P.; Fanjul, A.; Picard, N.; Shroot, B.; Pfahl, M. A selective retinoid with high activity against an androgen-resistant prostate cancer cell type. *Int. J. Cancer* **1999**, *80*, 272−278.
(102) Ponzanelli, I.; Gianni, M.; Giavazzi, R.; Garofalo, A.; Nicoletti, I.; Reichert, U.; Erba, E.; Rambaldi, A.; Terao, M.; Garattini, E. Isolation and characterization of an acute promyelocytic leukemia cell line selectively resistant to the novel antileukemic and apoptogenic retinoid 6-[3-adamantyl-4-hydroxyphenyl]-2-naphthalenecarboxylic acid. *Blood* **2000**, *95*, 2672−2682.
(103) Lovat, P. E.; Ranalli, M.; Bernassola, F.; Tilby, M.; Malcolm, A. J.; Pearson, A. D.; Piacentini, M.; Melino, G.; Redfern, C. P. Synergistic induction of apoptosis of neuroblastoma by fenretinide or CD437 in combination with chemotherapeutic drugs. *Int. J. Cancer* **2000**, *88*, 977−985.
(104) Lovat, P. E.; Ranalli, M.; Bernassola, F.; Tilby, M.; Malcolm, A. J.; Pearson, A. D.; Piacentini, M.; Melino, G.; Redfern, C. P. Distinct properties of fenretinide and CD437 lead to synergistic responses with chemotherapeutic reagents. *Med. Pediatr. Oncol.* **2000**, *35*, 663−668.
(105) Costantini, P.; Jacotot, E.; Decaudin, D.; Kroemer, G. Mitochondrion as a novel target of anticancer chemotherapy. *J. Natl. Cancer Inst.* **2000**, *92*, 1042−1053.
(106) Marchetti, P.; Mortier, L.; Beauvillain, V.; Formstecher, P. Are mitochondria targets of anticancer drugs responsible for apoptosis? *Ann. Biol. Clin. (Paris)* **2002**, *60*, 391−403.
(107) Buehler, C. A.; Harris, J. O.; Shacklett, C.; Block, B. P. The action of formaldehyde on *m*-hydroxybenzoic acid. II. *J. Am. Chem. Soc.* **1946**, *68*, 574−577.
(108) Kelly, K. G.; Ellenbogen, L. Histidine decarboxylase inhibiting 4-bromo-3-hydroxy-hippuric acid. Ger. Patent 2,062,611, 1971.
(109) Barrow, J. C.; Nantermet, P. G.; Selnick, H. G.; Glass, K. L.; Rittle, K. E.; Gilbert, K. F.; Steele, T. G.; Homnick, C. F.; Freidinger, R. M.; Ransom, R. W.; Kling, P.; Reiss, D.; Broten, T. P.; Schorn, T. W.; Chang, R. S.; O'Malley, S. S.; Olah, T. V.; Ellis, J. D.; Barrish, A.; Kassahun, K.; Leppert, P.; Nagarathnam, D.; Forray, C. In vitro and in vivo evaluation of dihydropyrimidinone C-5 amides as potent and selective α_{1A} receptor antagonists for the treatment of benign prostatic hyperplasia. *J. Med. Chem.* **2000**, *43*, 2703−2718.
(110) Case, D. A.; Pearlman, D. A.; Caldwell, J. W.; Cheatham, T. E., III.; Ross, W. S.; Simmerling, C. L.; Darden, T. A.; Merz, K. M.; Stanton, R. V.; Cheng, A. L.; Vicent, J. J.; Crowley, M.; Tsui, V.; Radmer, R. J.; Duan, Y.; Pitera, J.; Massova, I.; Seibel, G. L.; Singh, U. C.; Weiner, P. K.; Kollman, P. A. *AMBER6*. University of California, San Francisco, 1999.
(111) Ciccotti, G.; Ryckaert, J. P. Molecular dynamics simulation of rigid molecules. *Comput. Phys. Rep.* **1986**, *3*, 345.
(112) Goodsell, D. S.; Morris, G. M.; Olson, A. J. Automated docking of flexible ligands: Applications of AutoDock. *J. Mol. Recognit.* **1996**, *9*, 1−5.
(113) Morris, G. M.; Goodsell, D. S.; Halliday, R. S.; Huey, R.; Hart, W. E.; Belew, R. K.; Olson, A. J. Automated docking using a Lamarckian genetic algorithm and an empirical binding free energy function. *J. Comput. Chem.* **1998**, *19*, 1639−1662.
(114) Cornell, W. D.; Cieplak, P.; Bayly, C. I.; Gould, I. R.; Merz, K. M., Jr.; Ferguson, D. M.; Spellmeyer, D. C.; Fox, T.; Caldwell, J. W.; Kollman, P. A. A second generation force field for the simulation of proteins, nucleic acids, and organic molecules. *J. Am. Chem. Soc.* **1995**, *117*, 5179−5197.
(115) Bayly, C. I.; Cieplak, P.; Cornell, W. D.; Kollman, P. A. A well-behaved electrostatic potential based method using charge restraints for deriving atomic charges: The RESP model. *J. Phys. Chem.* **1993**, *97*, 10269−10280.
(116) Charpentier, B.; Bernardon, J. M.; Eustache, J.; Millois, C.; Martin, B.; Michel, S.; Shroot, B. Synthesis, structure-affinity relationships, and biological activities of ligands binding to retinoic acid receptor subtypes. *J. Med. Chem.* **1995**, *38*, 4993−5006.
(117) Sakashita, A.; Kizaki, M.; Pakkala, S.; Schiller, G.; Tsuruoka, N.; Tomosaki, R.; Cameron, J. F.; Dawson, M. I.; Koeffler, H. P. 9-*cis*-retinoic acid: Effects on normal and leukemic hematopoiesis in vitro. *Blood* **1993**, *81*, 1009−1016.
(118) Zhang, X.-K.; Hoffmann, B.; Tran, P. B.; Graupner, G.; Pfahl, M. Retinoid X receptor is an auxiliary protein for thyroid hormone and retinoic acid receptors. *Nature* **1992**, *355*, 441−446.
(119) Wu, Q.; Dawson, M. I.; Zheng, Y.; Hobbs, P. D.; Agadir, A.; Jong, L.; Li, Y.; Liu, R.; Lin, B.; Zhang, X.-K. Inhibition of *trans*-retinoic acid-resistant human breast cancer cell growth by retinoid X receptor-selective retinoids. *Mol. Cell. Biol.* **1997**, *17*, 6598−6608.

JM030524K